

A TIME SERIES ANALYSIS OF VOLCANIC DEFORMATION NEAR
THREE SISTERS, OREGON, USING INSAR

by

SUSAN NANCY RIDDICK

A THESIS

Presented to the Department of Geological Sciences
and the Graduate School of the University of Oregon
in partial fulfillment of the requirements
for the degree of
Master of Science

June 2011

THESIS APPROVAL PAGE

Student: Susan Nancy Riddick

Title: A Time Series Analysis of Volcanic Deformation near Three Sisters, Oregon,
Using InSAR

This thesis has been accepted and approved in partial fulfillment of the requirements for
the Master of Science degree in the Department of Geological Sciences by:

Dr. David A. Schmidt	Chair
Dr. Katharine V. Cashman	Member
Dr. Joshua J. Roering	Member

and

Richard Linton	Vice President for Research and Graduate Studies/Dean of the Graduate School
----------------	---

Original approval signatures are on file with the University of Oregon Graduate School.

Degree awarded June 2011

© 2011 Susan Nancy Riddick

THESIS ABSTRACT

Susan Nancy Riddick

Master of Science

Department of Geological Sciences

June 2011

Title: A Time Series Analysis of Volcanic Deformation near Three Sisters, Oregon,
Using InSAR

Approved: _____
Dr. David A. Schmidt

An extensive area west of the Three Sisters volcanoes of Oregon has been actively uplifting for over a decade. Examining the deformation is imperative to improve understanding of the potential hazards of Cascade volcanism and the emplacement of magma. I refine the timing of the onset of the deformation, resolve the change in uplift rates through time, and quantify the current deformation rate using Interferometric Synthetic Aperture Radar. The deformation is assessed in time and space using single interferogram InSAR, stacks of interferograms, and line-of-sight time series. I examine the shape of the deformation pattern and explore volcanic source parameters using a Mogi model and tension crack model with topographic corrections. By using the best fit model and combining all useable interferograms from different tracks, I create the first complete continuous inflation time series of the Three Sisters volcanic uplift from 1992 to 2010.

CURRICULUM VITAE

NAME OF AUTHOR: Susan Nancy Riddick

GRADUATE AND UNDERGRADUATE SCHOOLS ATTENDED:

University of Oregon, Eugene, OR
Cornell University, Ithaca, NY

DEGREES AWARDED:

Master of Science, Geological Sciences, 2011, University of Oregon
Bachelor of Science, Science of Earth Systems, 2009, Cornell University

AREAS OF SPECIAL INTEREST:

Remote Sensing
Geohazards

PROFESSIONAL EXPERIENCE:

Graduate Teaching Fellow, Department of Geological Sciences, University of Oregon, 09/2009-03/2011

Research Assistant, Department of Earth and Atmospheric Sciences, Cornell University, 06/2007-05/2009

NASA Undergraduate Student Research Program Internship, Jet Propulsion Lab, 06/2008-08/2008

New York NASA Space Grant Summer Research Program Internship, Cornell University, 06/2007-07/2007

Earth Science, Biology, and Math Tutor, Middletown High School, 06/2005-07/2005 and 06/2006-07/2006

GRANTS, AWARDS, AND HONORS:

Magna cum Laude, Cornell University, 2009

CALS Academic Excellence Award, Cornell University, 2009

Dean's List, Cornell University, 2005-2009

NYS TAP Scholastic Academic Excellence, 2005-2009

Elizabeth Collard Memorial Award, 2005

Nicholas Sylvester Scholarship, 2005

Middletown Women's University Club Scholarship, 2005

PUBLICATIONS:

Riddick, S. N., and D. A. Schmidt (2010), A Time Series Analysis of Volcanic Deformation near Three Sisters, Oregon, using InSAR, *Eos Trans. AGU*, Fall Meet. Suppl., Abstract G23C-0839.

Fournier, T. J., M. E. Pritchard, and S. N. Riddick (2010), Duration, magnitude, and frequency of subaerial volcano deformation events: New results from Latin America using InSAR and a global synthesis, *Geochem. Geophys. Geosys.*, 11, Q01003.

Pritchard, M. E., T. Fournier, S. Riddick, J. Jay, and S. T. Henderson (2009), The duration, magnitude, and frequency of subaerial volcano deformation events: New InSAR results from Latin America and a global synthesis, *Eos Trans. AGU*, Fall Meet. Suppl., Abstract V23D-2127.

Riddick, S., T. Fournier, and M. E. Pritchard (2009), Volcanic deformation in the Andes, *Eos Trans. AGU*, 90(22), Jt. Assem. Suppl., Abstract V33A-04.

Riddick, S. N., M. E. Pritchard, W. D. Barnhart, and R. B. Lohman (2008), Comparing C and L band InSAR observations of volcanic deformation in South America, *Eos Trans. AGU*, 89(53), Fall Meet. Suppl., Abstract G13B-0652.

Simard, M., N. Pinto, and S. Riddick (2008), Characterizing Vegetation 3D structure Globally using Spaceborne Lidar and Radar, *Eos Trans. AGU*, Fall Meet. Suppl., Abstract B41C-0402.

ACKNOWLEDGMENTS

I give my most sincere thanks to Dr. David Schmidt for the extensive amount of time he invested in helping and guiding me throughout the research process. I am forever grateful for the numerous skills I have gained as a result of his efforts. I would also like to thank Dr. Katharine Cashman and Dr. Joshua Roering for their enthusiasm, expertise, and valuable feedback that significantly improved this manuscript. I am very thankful for my friends and family, especially my husband, for their continual love and support. Most importantly, I thank God for giving me this opportunity, as well as the strength and wisdom to be able to complete this degree. SAR data was acquired through WInSAR, the Alaska Satellite Facility, and from Chuck Wicks at the USGS. Topodef was provided by Charles Williams.

TABLE OF CONTENTS

Chapter	Page
I. INTRODUCTION	1
Geologic Setting.....	1
Background.....	3
Objectives	6
II. DATA AND METHODS.....	8
InSAR	8
Modeling	10
Inflation Time Series.....	13
III. InSAR RESULTS	14
IV. DISCUSSION.....	24
Onset of Deformation	24
Modeling InSAR Stacks	28
Inflation Time Series.....	37
Volcanologic Interpretation	39
StaMPS Assessment.....	45
V. CONCLUSIONS.....	50
APPENDIX: ACRONYM TABLE	52
REFERENCES CITED.....	53

LIST OF FIGURES

Figure	Page
1. Study Area: Three Sisters Volcanic Center	2
2. Shaded Relief Image of the Three Sisters Area	11
3. T163 ERS Interferogram.....	15
4. T385 ERS Interferogram.....	16
5. Stacks of Interferograms from T113 and T385 ERS	19
6. Stack of Interferograms from T113 ENVISAT	20
7. Small-Baseline and GPS Time Series.....	21
8. StaMPS Results for T385 ERS	22
9. T113 ENVISAT StaMPS and Small-Baseline Time Series	23
10. T113 ERS Interferogram.....	25
11. StaMPS Epochs from T385 and T113 ERS.....	27
12. Model Results Plots	32
13. T385 ERS Stack used in Modeling.....	33
14. Model Results for T385 ERS.....	35
15. Predicted Model Differences	36
16. Aspect Ratios	37
17. Inflation Time Series.....	39
18. StaMPS and Stack Comparison	47
19. T113 ERS Persistent Scatterers	48
20. Field Photos	49

LIST OF TABLES

Table	Page
1. Mogi Model Results.....	28
2. Tension Crack Model Results.....	30
3. Ellipsoid Model Results.....	31

CHAPTER I

INTRODUCTION

Geologic Setting

The Three Sisters volcanoes are part of the Cascades, an active volcanic arc formed from the subduction of the Juan de Fuca and Gorda plates beneath the North American plate. The Quaternary Cascade volcanic arc extends about 1200km, from southern British Columbia to Northern California [Sherrod and Smith, 1990]. The Three Sisters volcanic center is located in the High Cascades of central Oregon (Figure 1) and includes a number of composite volcanoes, shields, and cinder cones. North Sister is a basaltic andesitic composite volcano on a broad shield base formed by long-lived effusive volcanism with activity dating from ~400ka to ~50ka [Taylor, 1981; Schmidt and Grunder, 2011]. South Sister, Middle Sister, and Broken Top are younger composite basaltic-andesitic to rhyolitic volcanoes with histories of explosive volcanism [Taylor, 1981; Scott et al., 2001]. However, most of the volcanic activity in the Cascades has not derived from composite volcanoes. The majority (67-90%) of the volcanic activity in this area is associated with mafic shields and cones that are distributed around the major composite volcanoes [Sherrod and Smith, 1990; Hildreth, 2007]. There are approximately 1500 Quaternary volcanoes in the Oregon Cascades segment, most of which are scoria cones, small shield volcanoes and fissure-fed lava fields, composed mainly of basaltic andesite [Hildreth, 2007]. The 90 km long Sisters segment contains at least 466 vents, making it one of the most densely populated vent areas in the world [Hildreth, 2007].

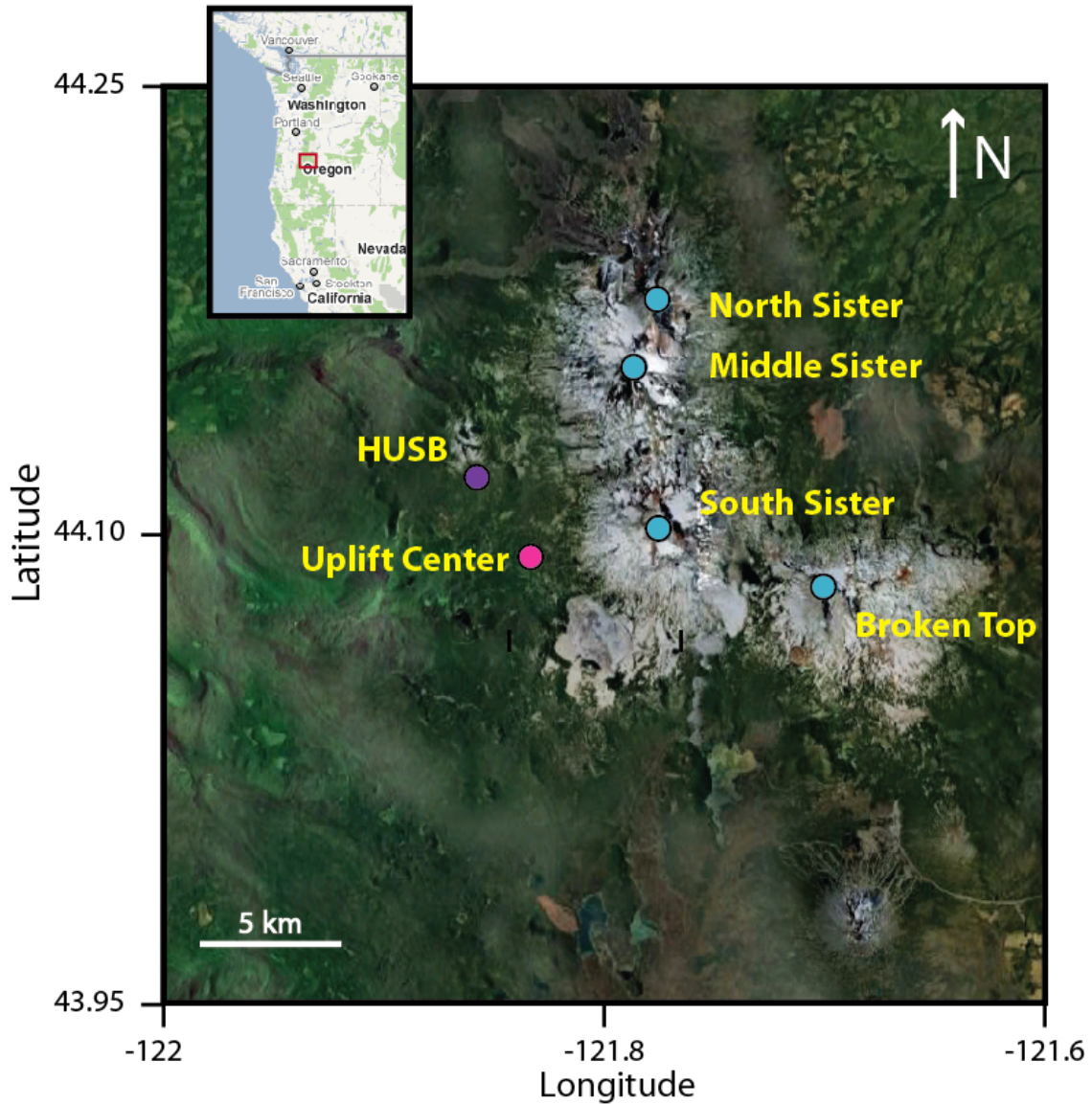


Figure 1. Study area: Three Sisters volcanic center, Oregon. Teal markers represent the main volcanoes, from north to south: North Sister, Middle Sister, South Sister, and Broken Top. The purple marker corresponds to the location of a continuous GPS station located at Husband, called HUSB. The pink marker represents the approximate center of uplift located ~5 kilometers west of South Sister.

Within the past 18ka, the total volume erupted from all vents within the Sisters segment is at least $30\text{-}50 \text{ km}^3$, with large uncertainties due to glacial erosion [Sherrod *et al.*, 2004; Hildreth, 2007]. The extrusion rate for central Oregon is higher than any other segment of the Cascade Range at $3\text{-}6 \text{ km}^3 \text{ km}^{-1} \text{ m.y.}^{-1}$ [Scott and Gardner, 1990]. The

Three Sisters volcanic center has been active within the past 2500 years. Approximately 2000 years ago South Sister produced two rhyolitic flank eruptions of lava, pyroclastic flows, and tephra fallout with a combined total volume of about 0.85 km^3 [Sherrod *et al.*, 2004; Hildreth, 2007]. Between 2 to 1.5ka, eruptions of basaltic to andesitic lava flows formed shield volcanoes and cinder cones near North Sister, such as Belknap crater, Four in-One-Cone, and Collier cone [Sherrod *et al.* 2004; Hildreth, 2007].

The central Oregon Cascades has a wide range of potential volcanic hazards, including fallout of tephra, lava flows, pyroclastic flows, landslides from the steep volcano flanks, and lahars [Scott *et al.*, 2001]. The USGS has determined that due to the high level of activity and range of volcanic hazards, the Sisters region should be continually monitored [Ewert *et al.*, 2005]. Concern about new activity and volcanic hazards in the Three Sisters region has grown since the discovery of volcanic uplift more than a decade ago [Wicks *et al.*, 2002]. This thesis expands the monitoring effort for the Three Sisters region by more fully documenting the time dependent uplift related to injection of magma at depth.

Background

Prior to 2001, the Three Sisters volcanic field was thought to be dormant. However in April 2001, Wicks *et al.* [2002] discovered a broad region of crustal uplift ~6km west of South Sister. The area has been continuously uplifting since that discovery. No significant seismicity has been associated with the inflation except for a swarm of 300 small magnitude earthquakes in March 2004 located in the northeast section of the deforming area [Moran, 2004]. One deep long-period (DLP) earthquake was identified at

~12km depth beneath the Three Sisters deforming area in 2006; DLPs are commonly associated with the presence of magma [Nichols *et al.*, 2011]. The Three Sisters deformation has been attributed to an intrusion of magma at depth [Dzurisin *et al.*, 2009]. The most recently published best-fit model to the deformation data is a vertical, prolate, spheroidal point-pressure source at 4.9-5.4 km depth [Dzurisin *et al.*, 2009].

Interferometric Synthetic Aperture Radar (InSAR) has been the main method to study the Three Sisters deformation. InSAR is a remote sensing technique that utilizes satellites to study ground deformation with millimeter precision [e.g., Rosen *et al.*, 2000]. This technique has a variety of applications, but most pertinent to this study is its application to the identification and quantification of volcanic deformation. By interfering the radar chirps backscattered from the surface from two different satellite passes, one can measure the phase change of the signal related to the surface deformation over a period of time [e.g., Rosen *et al.*, 2000]. InSAR is the principal technique used to study the inflation near the Three Sisters volcanoes because of the difficulties in installing ground-based geodetic and seismic instrumentation in a wilderness area.

When using InSAR to study deformation in the Three Sisters area, the greatest challenge is the decorrelation of the radar signal related to vegetation and snow. Phase decorrelation in interferograms is created when neighboring pixels do not have similar phase values, or are not spatially correlated [Zebker and Villasenor, 1992]. In the Three Sisters area, this is caused primarily by dense vegetation or snow, either of which can significantly change the backscatter characteristics of the ground over short periods of time. The high variability in time and space gives rise to decorrelated patches in

interferograms. For this reason, correlated areas of interferograms in the Three Sisters region are limited mainly to the sparsely vegetated lava flows.

The degree of decorrelation is also dependent on the wavelength of the radar signal used by the satellite. C-band radar has a wavelength of 5.6 cm, which cannot easily penetrate vegetation such as shrubs or grass. L-band has a longer wavelength of 23.6 cm, which is able to better penetrate vegetation and backscatter off of the stable bedrock surface. Thus L-band data would be the best choice to obtain a more complete deformation pattern. However, L-band data is less precise than C-band, making it more difficult to detect small signals. Additionally, L-band data is available only from 2006 to present from the ALOS satellite. Unfortunately, the Three Sisters deformation rates from 2006 through present are too small to be detected by L-band (Chapter III). As a result, the L-band data show no significant or detectable deformation. Thus, my analysis focuses on the C-band radar data acquired by the ERS and ENVISAT satellites operated by the European Space Agency (ESA).

Decorrelation of C-band data, and inability to obtain information from ALOS L-band data, requires that other techniques must be used to obtain a more spatially complete deformation pattern. One such technique is StaMPS, an algorithm that identifies surface scatterers (buildings, rock outcrops, etc.) with stable radar characteristics that are called persistent scatterers [e.g., *Hooper et al.*, 2007; *Hooper*, 2008]. The phase is acquired only on those points, which allows the deformation signal to be recovered from some areas that were decorrelated in single interferograms. By using a variety of techniques such as StaMPS, single interferogram InSAR, stacks of interferograms, and time series of small-baseline interferograms, I examine the Three Sisters deformation in time and space.

Objectives

My primary motivation for this study is to better quantify the magmatic inflation source beneath the Three Sisters area. In a broader sense, this work will improve understanding of the life cycle of volcanic systems and mechanism of recharge between major eruptions. I model InSAR data to determine the source geometry that best describes the uplift (point source, ellipsoidal magma chamber, or tension crack representing a sill-like intrusion). The model solves for the depth of the source and the rate of volume change. By using the model that best fits the data, I create an inflation time series of the deformation. Modeling and time series results help with hazard assessment as well as improve comprehension of non-eruptive volcanic activity and the behavior of current volcanism in the Cascades.

A main objective of this study is to fill in all data gaps from previous publications and present the first InSAR line-of-sight (LOS) time series of the Three Sisters deformation. Previous publications do not present the deformation rate from 2006 to present or provide yearly deformation rates from 2001-2006 [Wicks *et al.*, 2001; Dzurisin *et al.*, 2006 and 2009]. To fill in all data gaps and determine the current deformation, all available ERS and ENVISAT InSAR data from 1992-2010 are processed. With the InSAR data, LOS time series are created to help determine how the onset of deformation began and at what rate, how the deformation changed through time, and whether the deformation is still occurring.

Another goal is to more precisely determine the onset of deformation. Wicks *et al.* [2002] conclude that most if not all of the early uplift occurred between September 1998 and October 2000, based on the analysis of individual interferograms. Dzurisin *et al.*

[2006] state that the deformation began between the summer of 1996 and the summer of 1998. They determine this time range by using a scaling factor to relate tilt-leveling results to predicted Mogi model results, as well as the assumption that the uplift was steady since inception. *Dzurisin et al.* [2009] use a model derived from GPS and leveling data to extrapolate back to an onset of September of 1997. Because such a range of start times exist, I analyze the InSAR data in detail with several methods to arrive at a precise time of onset derived solely from InSAR, which is the only dataset that spans the entire period. The inception of deformation is helpful for hazard assessment and risk mitigation. Examining the transition from dormancy to renewed activity can help with the earlier identification of newly reactivating volcanoes, especially those volcanoes that are aseismic and do not present other indicators of activity besides surface deformation.

A further goal is to assess how well StaMPS performs in the Cascades, since the technique has not been implemented in this area before. The dense vegetation of the western Cascades causes partial to complete decorrelation over the uplifting region. However, StaMPS should be capable of finding persistent scatterers on rocky outcrops within vegetated areas that would be completely decorrelated with single interferogram InSAR. I evaluate the accuracy of StaMPS by the chosen scatterers' locations relative to ground features as well as comparing StaMPS time series results to other InSAR method results.

CHAPTER II

DATA AND METHODS

InSAR

I process ERS, ENVISAT, and ALOS SAR data to create single interferograms. A 30-meter resolution DEM produced from SRTM tiles covering the Three Sisters area is used to remove topographic contributions to the phase in interferogram processing [Farr and Kobrick, 2000]. Orbit files are used to estimate and remove the orbital error. I utilize JPL/Caltech ROI PAC software to process the SAR data and create interferograms [Rosen et al., 2004], as well as a Stanford package called SNAPHU to unwrap interferograms [Chen and Zebker, 2002]. Default parameters are used in ROI PAC and SNAPHU, including processing the SAR data at four looks. Only interferograms with perpendicular baselines of 500m or less are processed. Interferograms with baselines higher than ~500m are normally too incoherent to detect deformation. Furthermore, only summer and early fall SAR scenes are considered in my analysis due to snow cover in the Cascades. Given these data constraints, I processed ~800 interferograms covering the Three Sisters area and analyzed these data with a variety of complementary methods.

Atmospheric artifacts resulting from the heterogeneous distribution of water vapor in the atmosphere is the greatest source of error in individual interferograms. To minimize this error source and resolve the deformation signal, I stack interferograms [e.g., Zebker et al., 1997; Sandwell and Price, 1998]. The method stacks and averages the deformation for each stacked pixel over the entire time spanned by the interferograms. This gives an average range change rate. With enough interferograms stacked, random noise will cancel, creating a more accurate map of the deformation.

An InSAR time series inversion developed by *Schmidt and Bürgmann* [2003] is also implemented with single interferograms. The method linearly inverts independent unwrapped interferograms. Only the most coherent interferograms with little to no atmospheric or topographic errors are utilized. I use interferograms that have perpendicular baselines of ~150m or less. I also choose to have a small amount of smoothing (0.1 out of 1) and average the range-change over a radius of 3 pixels. The small-baseline time series determines the amount of deformation in each epoch between SAR acquisition dates. The time series provides the average deformation of the uplifting region relative to a stable area far from the deformation.

Andy Hooper's StaMPS version 3.2b3 is implemented to study the Three Sisters deformation [*Hooper et al.*, 2007; *Hooper*, 2008]. With the persistent scatterer (PS) method, one can create an image of the phase change on the most stable scatterers. There are several advantages to using StaMPS. StaMPS is a PS technique that accurately determines PS pixels in rural locations. Other persistent scatterer techniques are more successful in urban environments [e.g, *Ferretti et al.*, 2000, 2001]. StaMPS is able to identify stable ground scatterers, such as large boulders or lava flows within vegetation, by using spatial correlation of interferometric phase to find and select pixels with low phase variance [*Hooper et al.*, 2007]. Whereas the phase information in single interferograms is completely lost when there are neighboring incoherent pixels, StaMPS can identify the stable scatterers within incoherent patches and extract the phase information at those points. The final output of StaMPS is a time series showing cumulative deformation. This time series is made from persistent scatterer pixel interferograms coregistered to one master with various errors removed. The time series

results from StaMPS are compared directly with the small-baseline time series discussed in the previous paragraph. I use default parameters during StaMPS processing and chose the final product be the unwrapped phase with the DEM, orbit, and atmospheric error removed.

Modeling

I model the Three Sisters deformation to better understand the magmatic source, the behavior of volcanic systems in time, and the recharge of magma between major eruptions. A Mogi model, tension crack model, and ellipsoid model are all implemented to determine the best fit to the data [*Mogi, 1958; Yang and Davis, 1986; Davis, 1986*]. I model separate stacks of interferograms for each satellite track and solve for tilts and offsets that may be caused by orbital ramps that were not successfully removed during interferogram processing. Due to significant topography in the Three Sisters region, the models include a topographic correction that accounts for how the topography affects the deformation signal in regions of high relief (Figure 2) [*Williams and Wadge, 2000*]. Green's functions that relate the surface deformation to the inflation of a buried source in an elastic half-space are calculated using *Williams and Wadge's* [2000] package, Topodef. I utilize Topodef because the higher-order corrections more accurately account for topographic effects compared to a simple first-order correction [*Williams and Wadge, 1998*]. Deformation models for an inflation source show a tradeoff between volume change and depth. Thus, I iteratively optimize the volume change while varying the depth in 20m increments. Although a depth spacing of less than 20m would be ideal, the inversion would be too time intensive for each track and each model if run at a higher

depth resolution. Jackknifing of the stacks was also implemented to determine the sensitivity of the model to data variability [e.g., *Miller, 1974*]. For the jackknifing, one interferogram was taken out from each stack at a time and the model was rerun iteratively.

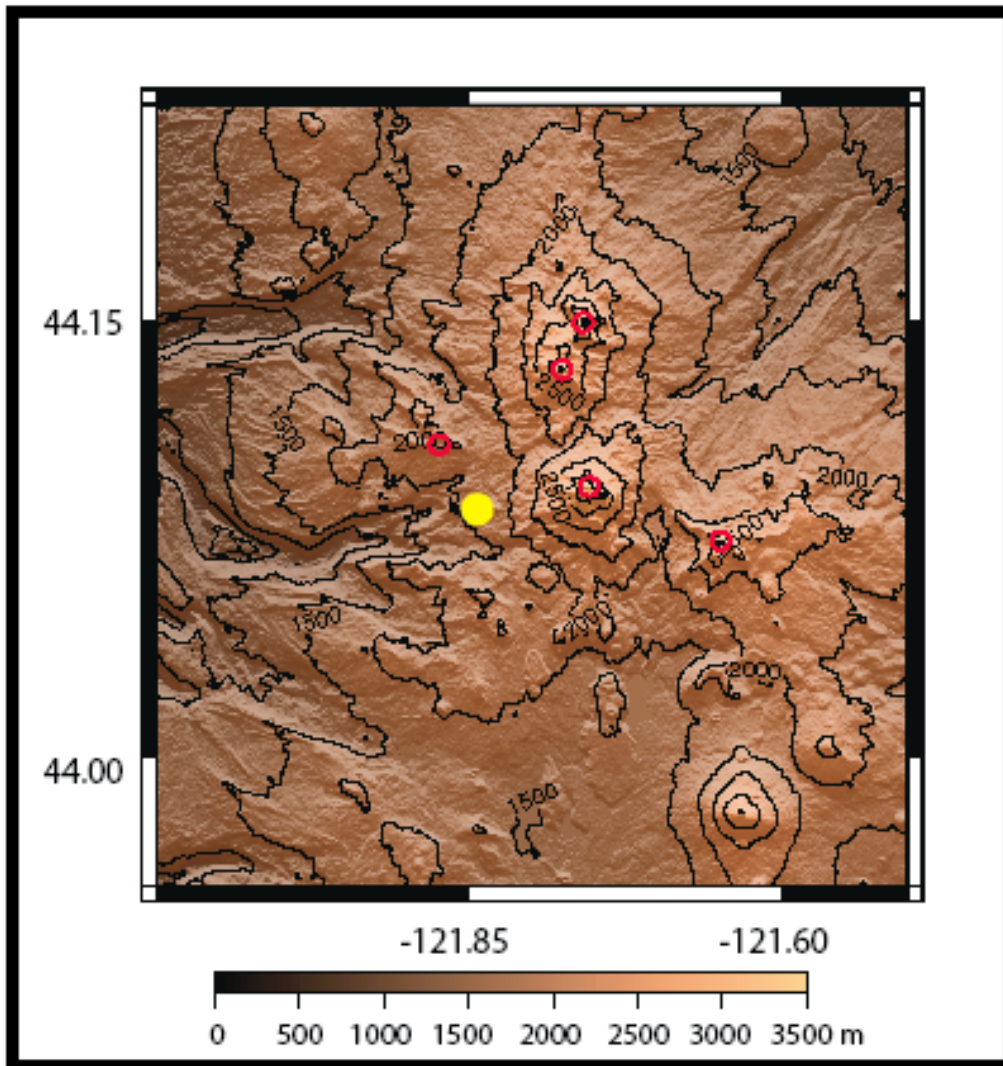


Figure 2. Shaded relief image of the Three Sisters area. Red circles correspond to volcanoes and GPS station HUSB from Figure 1. Yellow marker is the approximate center of the deformation. Elevation ranges from <1000m to over 3000m. South Sister is the highest in elevation at 3157m. The contour interval is 250 m.

The most basic and commonly used magmatic inflation model is the Mogi model, a point pressure source in an elastic half space [Mogi, 1958]. Due to the relative ease of setup, I begin with this model. I also implemented a tension crack model to determine the best fit for a dike or sill-like source [Yang and Davis, 1986]. Preliminary modeling showed that a vertical dike would not fit the data, and so I did not pursue a dike any further. The horizontal crack model was used as an approximation of a sill. An aspect ratio of length/thickness of the sill was selected as 1000, and the width of the sill was assumed to be the same as the length due to the symmetry of the deformation signal. The reasoning for the preference of a 1000 aspect ratio is described in more detail in Chapter IV, which explains how the ratio is a compromise between field data, experimental data, and inverse modeling. By fixing the aspect ratio, I reduce the number of free parameters in the model and thereby keep the analysis time of the iterative inversion scheme to a reasonable level. The crack model solves for depth and a volume change rate. The length (and width) and opening can be calculated from volume change based on the aspect ratio. Furthermore, I model the source with an ellipsoidal source [Davis, 1986]. The ratios of the three axes were solved for and depth was iterated in 20m increments using the best axis ratios for each track. Jackknifing was implemented on the stacks, although instead of calculating aspect ratios for each run, I used the best aspect ratio from the appropriate track's stack. This was necessary due to the very large number of Green's functions that would be required, which would be exceedingly time intensive.

Inflation Time Series

While the small-baseline time series provides a record of the surface deformation from individual satellite tracks, I also produce a time series of the inflation source utilizing all of the quality interferograms in a combined inversion. ERS data provides yearly SAR acquisitions from 1992 through 2008 with multiple year gaps of no useable data due to gyroscope malfunctions of the satellite. ENVISAT SAR data only spans 2003 through the present. Because each satellite and each track's data have different SAR acquisition dates, and only summer and fall data can be used, time series for each track are sparse with large gaps in time. Because there is a sufficient amount of data from both satellites and all tracks combined, it would be ideal to create a time series utilizing all the data. In order to do this, an inflation time series is needed to combine data of different look angles to a look-angle independent term such as pressure or volume change of a source. With the best fit model, a continuous inflation time series is made combining all useable interferograms of different satellite geometries. Using the least-squares formulation of *Grandin et al.* [2010], I create the source inflation time series constrained by the best single interferograms, i.e., those interferograms with good coherence, small perpendicular baselines, and minimal atmospheric artifacts. With the average depth from the best fit model from the previous section, I create a time series of the inflation for each SAR acquisition date from 1992-2010.

CHAPTER III

InSAR RESULTS

I process more than 800 ERS, ENVISAT, and ALOS interferograms from seven ascending and six descending satellite tracks. Deformation rates are obtained from 1992 through 2010. Only ~15% of the C-band interferograms processed for each track are sufficiently coherent to be used in stacking, and ~8-10% of the C-band interferograms are useable for the small-baseline inversion. The low number of coherent C-band interferograms highlights the challenge of using InSAR with the dense vegetation of the Cascades. Although C-band interferograms of the Cascades are generally decorrelated, some are surprisingly coherent and fully image the deformation west of South Sister (Figure 3, Figure 4).

The observed deformation is a broad ~20km-by-30km area with the North-South extent spanning from ~5km south of Belknap crater to the latitude of Mount Bachelor, and the East-West extent ranging from Broken Top to ~15km west of the peak of South Sister. The center of maximum uplift is located approximately ~5km west of the peak of South Sister. The SAR satellites record an increase in the LOS range change, which corresponds to uplift of the ground if all deformation is assumed to be vertical. The deformation pattern is not perfectly symmetrical, with a slight extension of the signal about 10-20 degrees clockwise from North. The fringes are generally equally spaced implying a roughly linear decrease in the LOS rate as one moves from the center of the deformation pattern. The coherence is good in the summer and fall for the High Cascades where there is less vegetation, but coherence decreases rapidly over the Western Cascades which are densely forested.

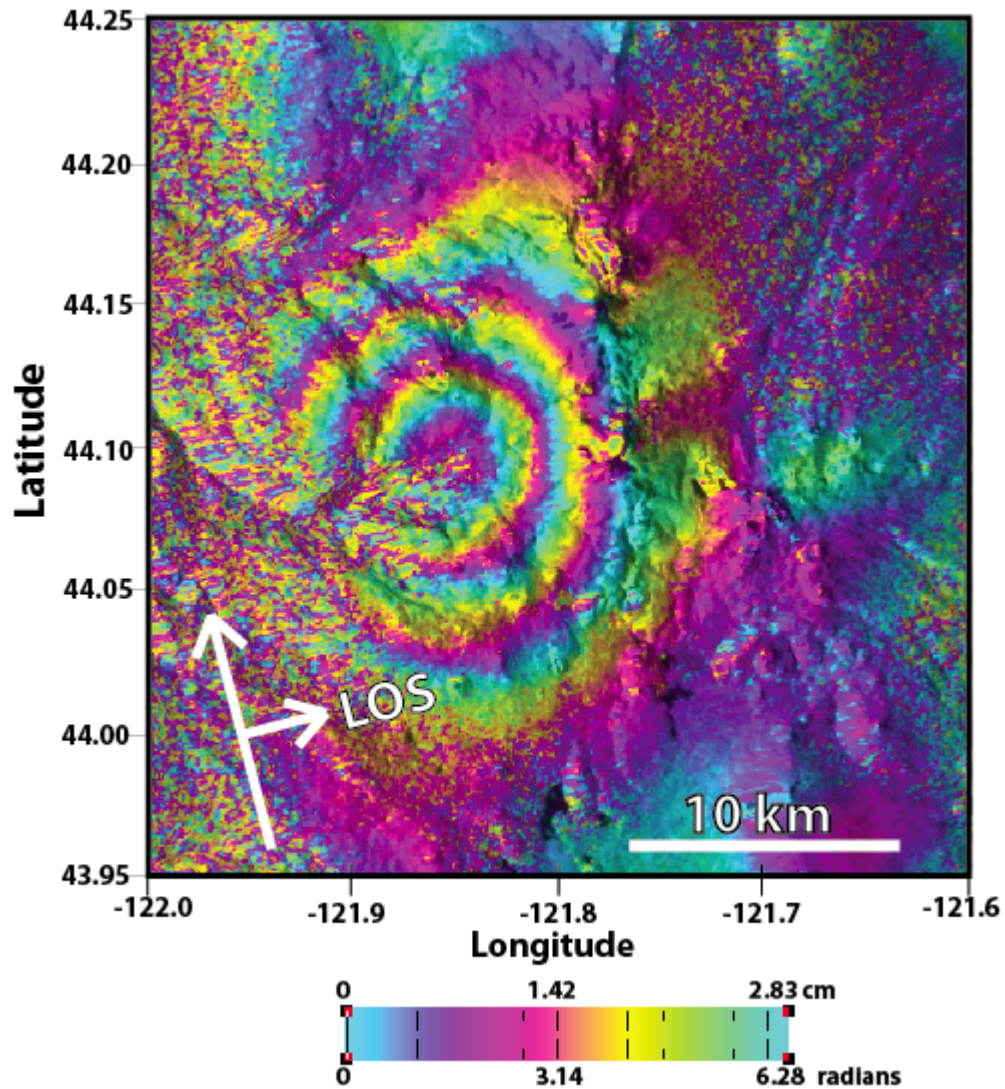


Figure 3. T163 ERS interferogram. An exemplary wrapped interferogram showing as much as 8cm of LOS surface deformation along Track 163 of the ERS satellite. The interferograms covers a nearly 4-year period from October 7th 2000 to October 16th 2004. Arrows indicate the LOS look direction (to the ENE) and the flight path of the satellite (to the NW).

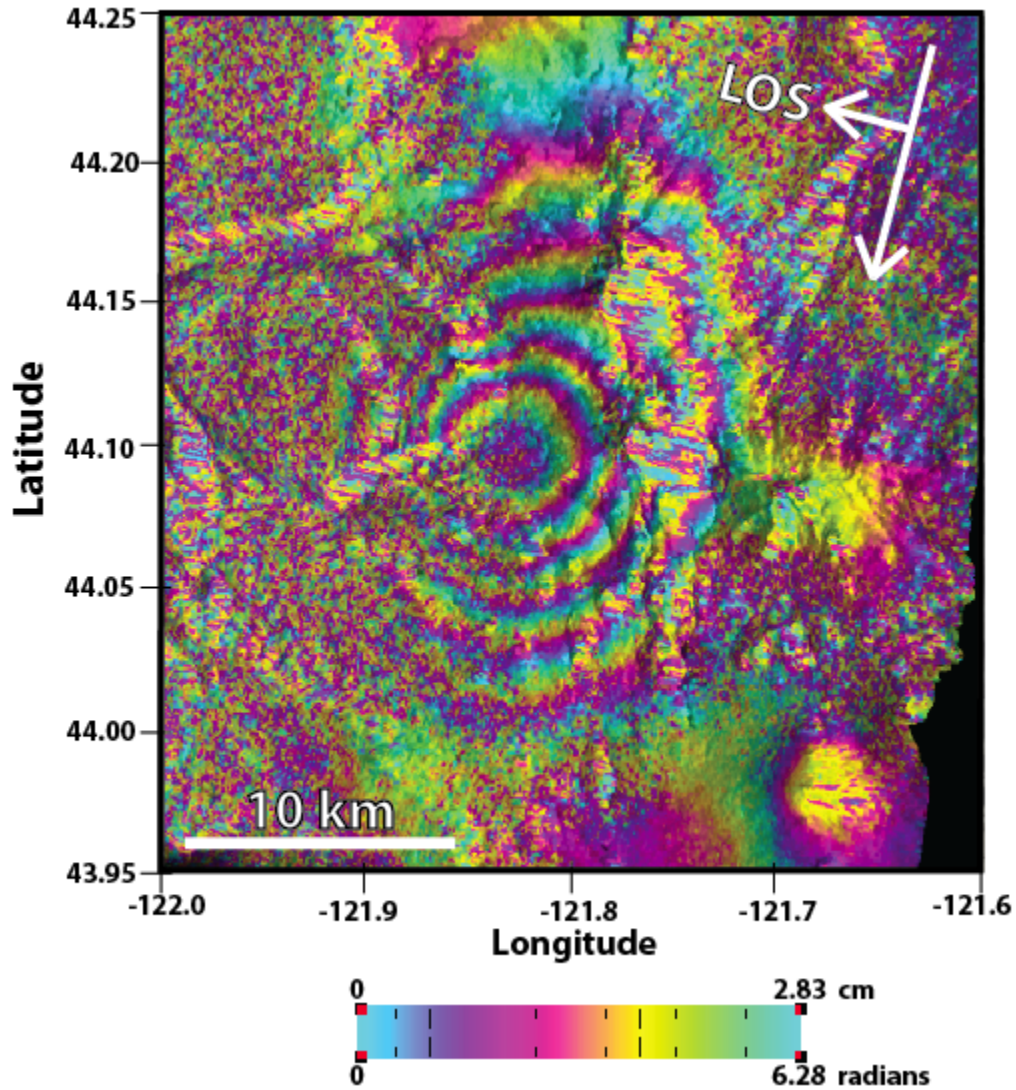


Figure 4. T385 ERS interferogram. A wrapped interferogram showing as much as 15cm of LOS surface deformation along Track 385 of the ERS satellite. The interferogram spans nearly a 5-year period from September 13th 1998 to September 7th 2003. Arrows indicate the LOS look direction (to the WNW) and the flight path of the satellite (to the SW).

Stacking interferograms helps to refine the deformation pattern by damping random noise. Stacking different subsets of interferograms reveals no deformation from 1992-1995, some deformation between 1995 to August 1997, and significant deformation after 1997 (Figure 5). The 2010 LOS rate is small, on the order of several millimeters to one centimeter per year. Single interferograms do not show a clear signal, but all three ENVISAT stacks show average LOS rates of ~6-8 mm/yr from 2006 to 2010 (e.g., Figure 6). The stacks show a slight bend in the phase contours around South Sister. This deflection is expected because the high topographic relief should distort the surface deformation.

The InSAR time series help to image the time dependent evolution of the deformation. The small-baseline time series reveals a gradual start to the deformation of ~1cm/ yr, which then increases to a maximum uplift rate of 3-4.5 cm/yr from 1998 through 2003 (Figure 7). After the summer of 2003, the deformation rate decreases. StaMPS time series confirm these results with similar trends of LOS range-change (Figure 8, Figure 9). The total amount of LOS range-change from the onset through 2010 is approximately 25 cm. All ENVISAT StaMPS time series also show potential current deformation through 2010 (e.g., Figure 9). There is also good agreement between the small-baseline time series and GPS time series. GPS data from a continuous station near the uplift (HUSB station on Figure 1) was projected onto the T385 ERS LOS time series to directly compare with the InSAR results (Figure 7). The GPS time series suggests a small amount of deformation occurring in 2010. The individual components of the GPS data, however, show that the deformation at the station is not purely vertical, but is moving north with an average rate of about 1cm/yr and west at a few mm/yr relative to

stable North America. This horizontal movement is largely related to the regional rotation and northward translation of the Oregon forearc [McCaffrey *et al.*, 2000]. However, the decay in velocity is representative of the local deformation near South Sister.

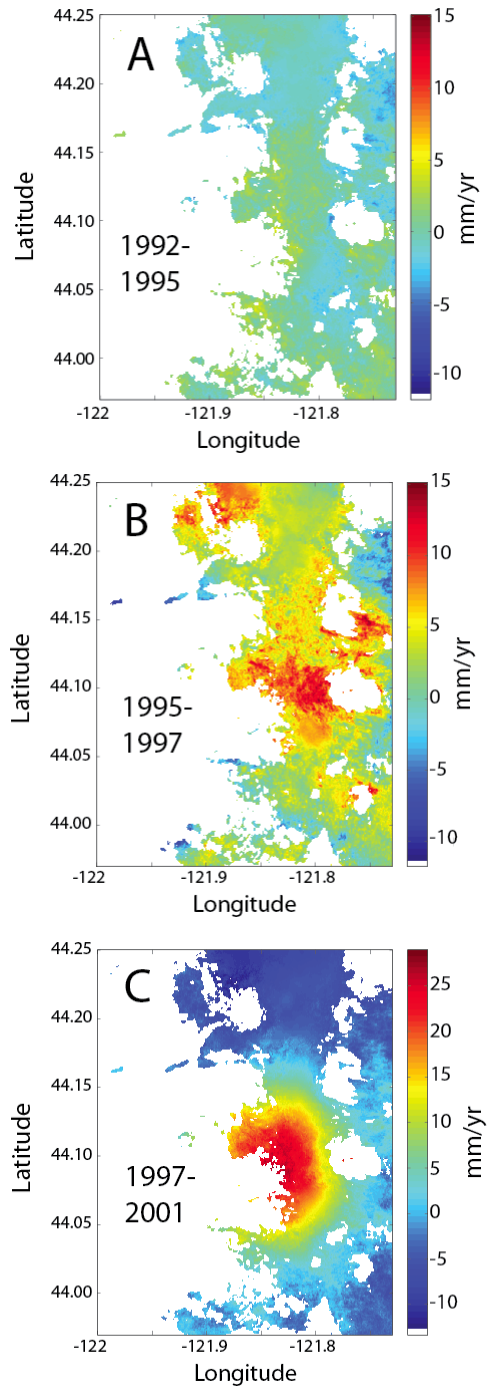


Figure 5. Stacks of different subsets of interferograms from T113 and T385 ERS. LOS range change is back-projected onto vertical. Note that A and B have the same scale while C is a different scale. A) Stack of 15 interferograms spanning June 13th 1992 to November 13th 1995. No signal is seen; B) Stack of 8 interferograms spanning July 31st 1995 to August 24th 1997. The start of a signal is observed in this epoch; C) Stack of 11 interferograms spanning August 24th 1997 to October 7th 2001. A signal is clearly seen in this stack.

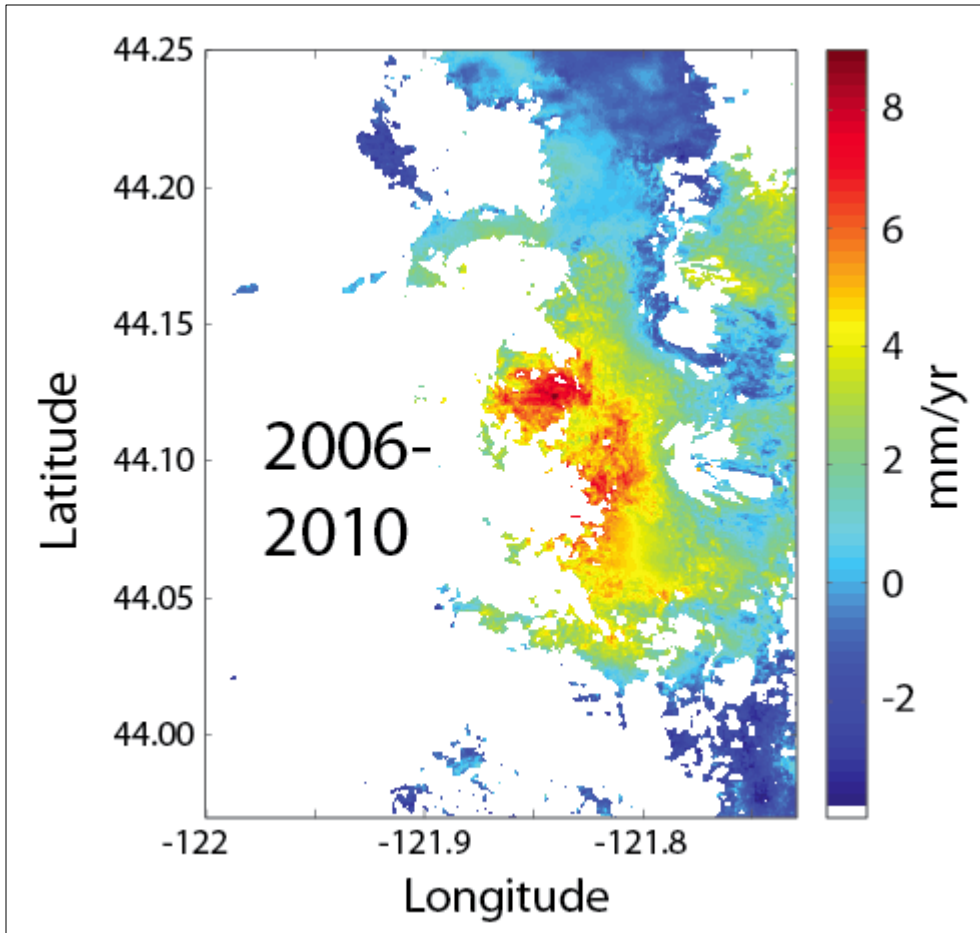


Figure 6. A stack of 11 interferograms from T113 ENVISAT, spanning 2006 through 2010 with a maximum rate of ~6-8mm/yr.

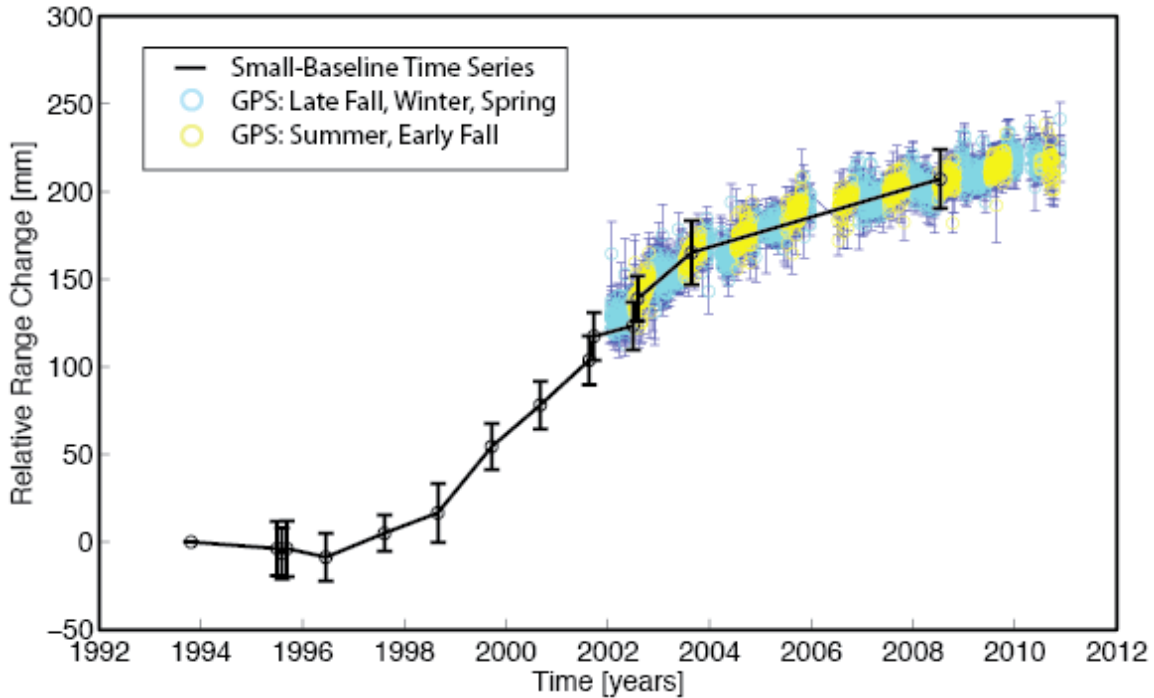


Figure 7. Small-baseline time series of T385 ERS interferograms (black) and GPS time series (blue and yellow). The small-baseline time series represents an average of neighboring pixels centered over the area of greatest range-change. Positive LOS range-change starts gradually after June 30th 1996 with the rate increasing through 2003 and then decreases. Black error bars represent the scatter in phase. Continuous GPS data is available after 2002. Daily GPS position (cyan and yellow circles) from station HUSB (purple marker on map in Figure 1). The vertical, north, and east components are projected onto the line-of-sight for T385 ERS. Yellow colored circles correspond to the summer and fall for a direct comparison to InSAR. Cyan circles represent snow-covered months. Dark blue error bars are calculated based on the error of all three GPS components. GPS data and errors were obtained from the Pacific Northwest network on the USGS website. The GPS plot agrees well with the small-baseline InSAR time series from 2002 through 2008.

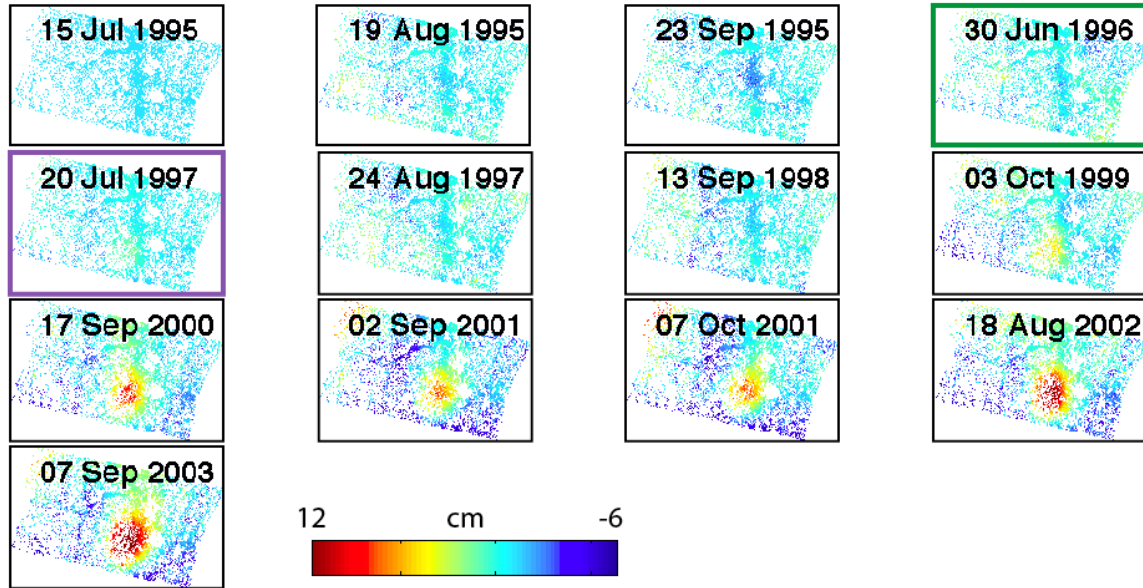


Figure 8. StaMPS results for T385 ERS. Each image shows cumulative LOS range-change with reference to the first scene of July 1995. The green and purple boxes correspond to Figure 11. The region shown in each frame is roughly similar to Figure 1.

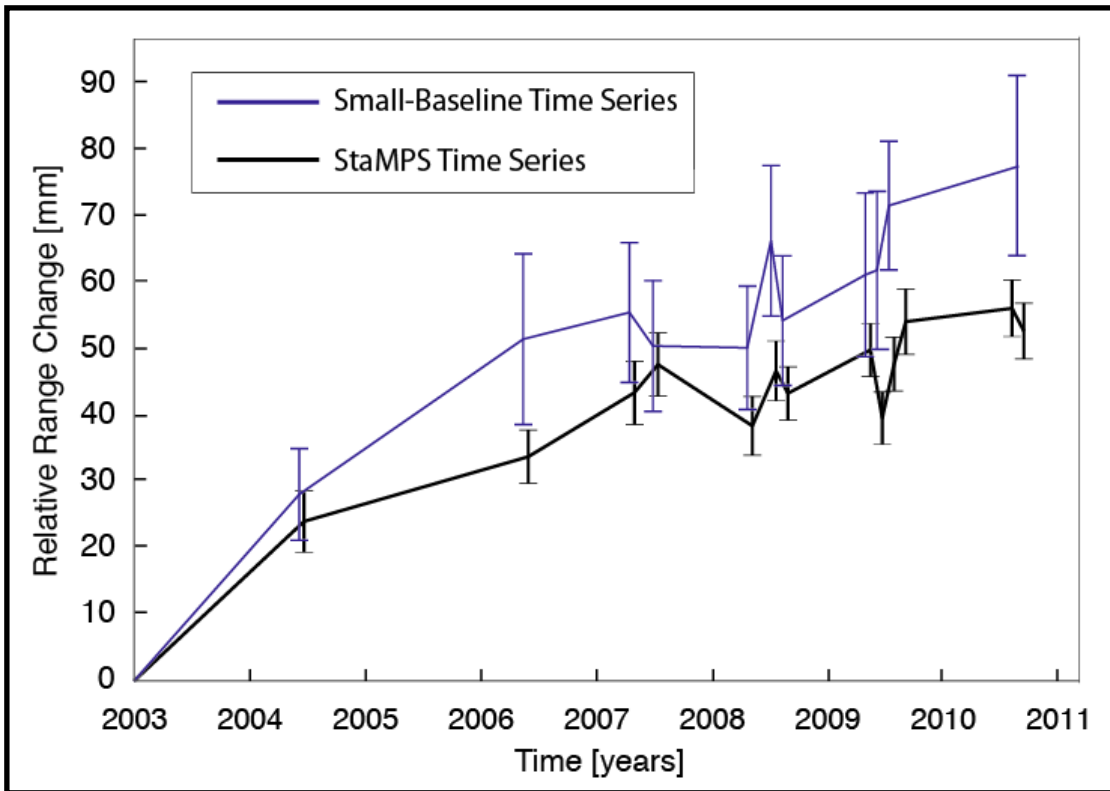


Figure 9. T113 ENVISAT StaMPS and small-baseline time series. Both show the general decrease in LOS range-change from 2004 through 2010. The difference in magnitude of the two time series is likely related to the different size of areas used in averaging the range-change and a different reference frame.

CHAPTER IV

DISCUSSION

Onset of Deformation

Determining the onset of deformation is important for hazard assessment because it shows how volcanoes transition from dormancy to activity. To determine the inception of activity, I analyze single interferograms, stacks, small-baseline time series, and StaMPS time series. By analyzing results from these methods, I determine the onset of the deformation to be between August 1996 and July 1997. This is earlier than prior extrapolation from a model derived from leveling and GPS data [Dzurisin *et al.*, 2009].

To determine the time of onset, I first analyzed single interferograms. Single interferograms do not provide an exact onset date because some interferograms do not show deformation, are completely incoherent or show noisy potential deformation (Figure 10). This explains why previous researchers could not give a more specific time period for the onset based on the interferograms. Thus, other methods are needed to help determine the initiation of deformation.

To improve the signal to noise ratio, I use my InSAR stacks to find a small signal that is spatially consistent through time. Three stacks of different time periods are used to identify the onset: 1992-1995, 1995-1997 (before September), 1997-2001 (Figure 5). These stacks combine data from two different satellite tracks. To combine the data with different look angles, the deformation is assumed to be only vertical. By combining the two tracks, spatially consistent signals in both tracks will add. Using this method the onset of deformation can be identified by the presence of a spatial pattern. The stack for

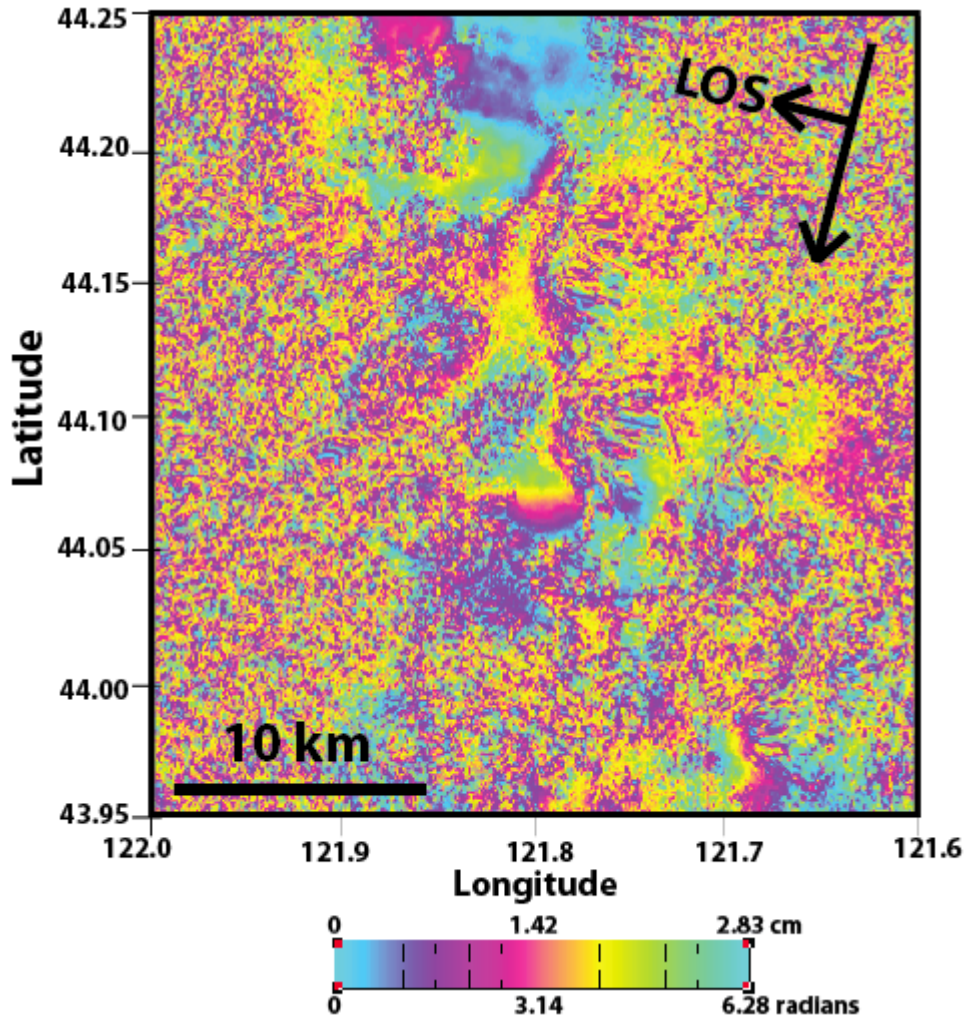


Figure 10. T113 ERS interferogram. This unwrapped interferogram from Track 113 ERS is the best interferogram to capture the onset of deformation. It covers nearly a 5-year period from September 26th 1992 to August 5th 1997 and potentially shows <3cm of deformation centered near the region of uplift. However, the interferogram is mostly incoherent with a large amount of noise. The region shown is identical to Figure 3.

1992-1995 shows no deformation. Stacked interferograms spanning 1995-1997 reveal the beginning of a spatial pattern west of the Sisters. Data stacked from 1997-2001 show a clear signal, with a prominent bulge.

The inception of deformation can also be estimated from my InSAR time series. Inspecting the individual epochs of my StaMPS results for T385 ERS (Figure 8), one can see no uplift occurring in the June 1996 epoch (Figure 11 A) but there is an uplift signal in the July 1997 epoch (Figure 11 B). Both epochs are referenced to the first date shown in Figure 8. Because the June 1996 image shows no deformation, this implies that the deformation in the July 1997 image must have occurred between June 30th 1996 and July 20th 1997. The small-baseline inversion for T385 ERS data confirms that the deformation began between June 30th 1996 and July 20th 1997 (Figure 7). Similarly, this is seen in StaMPS T113 ERS, which reveals that deformation started between August 20th 1996 and August 5th 1997 (Figure 11 C and D). Using information from both tracks, this implies an onset of deformation between August 20th 1996 and July 20th 1997. Although the time of onset given here is limited by the SAR acquisitions and the seasonal effects of snow, it is as tightly constrained as possible with InSAR. If the area of study was in a locality with little to no snow, the onset of deformation could be narrowed to within a few months.

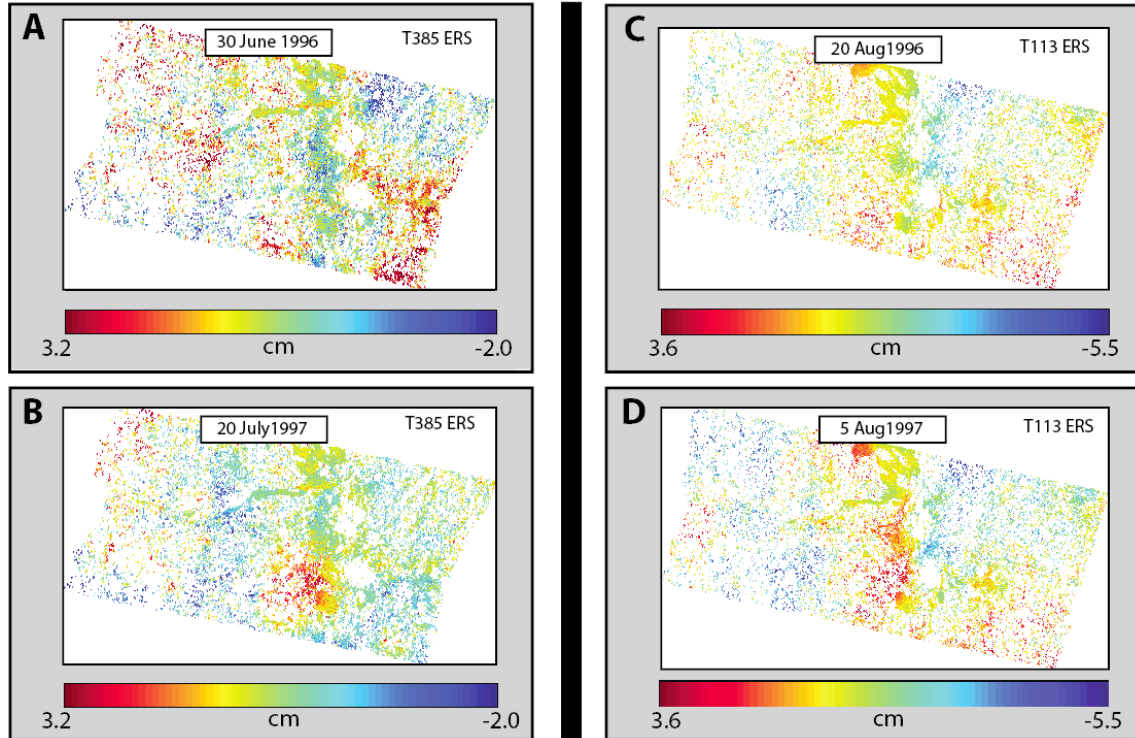


Figure 11. Individual StaMPS epochs from T385 and T113 ERS. A) Green box in Figure 8 of StaMPS T385 ERS time series. Deformation from July 15th 1995 to June 30th 1996. No deformation is observed over the uplift area; B) Purple box in Figure 8 of StaMPS T385 ERS time series. Deformation from July 15th 1995 to July 20th 1997 shows a circular uplift pattern west of South Sister. Since A shows that no deformation occurred through June 30th 1996, this implies that the uplift must have started between June 30th 1996 and July 20th 1997. C) A similar onset of deformation is seen in StaMPS for T113 ERS. The figure shows no significant deformation from August 22nd 1992 to August 20th 1996. D) Deformation from August 22nd 1992 to August 5th 1997. Although the onset in the cumulative epochs is not as clear as A and B of T385 ERS, viewing the incremental images (not shown) clearly shows the onset in the August 20th 1996 to August 5th 1997 epoch. C and D are also noisier because atmospheric error was not subtracted from the signal and thus propagated through the time series. Atmospheric error was not taken out because the error mapped in most of the deformation signal, and thus subtracting the atmosphere would also take out the signal. Using the StaMPS information from T385 ERS and T113 ERS, deformation likely began between August 20th 1996 and July 20th 1997. The region shown in each frame is roughly similar to Figure 1.

Modeling InSAR Stacks

The deformation resolved by InSAR is indicative of a pressurized magma source at depth. As a first-order exploration of the inflation source, a Mogi model is considered due to the relatively symmetrical shape of the ground deformation [Mogi, 1958]. Using the InSAR stacks, I iteratively invert for the optimal volumetric inflation rate while varying source depths. The Mogi model gives source depths that range from ~4-5.5 km with volume change rates of $\sim 2-4 \times 10^{-3} \text{ km}^3/\text{yr}$ (Table 1, Figure 12 A). The model fits the data extremely well based on the residuals (Table 1, Figure 13, Figure 14 A and B). The range of values in the tables signify model sensitivity to data variability from jackknifing of the stacks. Not surprisingly, the tracks with the least number of interferograms in the stacks have greater variability in depth and/or volume change rates.

Table 1. Mogi Model Results. Brackets indicate entire range of values from jackknifing. Parentheses indicate the number of interferograms used for each track.

Track	Volume Change Rate [km^3/yr]	Depth [m]	RMSE [m]
113 ERS (30)	0.00195 [0.00191, 0.00215]	3960 [3820, 4180]	0.000725 [0.000643, 0.000758]
113 ENVI (16)	0.00168 [0.00151, 0.00190]	4760 [4320, 5220]	0.000873 [0.000826, 0.000962]
385 ERS (37)	0.00379 [0.00355, 0.00392]	5220 [5100, 5340]	0.000628 [0.000617, 0.000650]
385 ENVI (16)	0.00194 [0.00168, 0.00236]	5480 [5040, 6160]	0.000620 [0.000603, 0.000671]
163 ERS (5)	0.00253 [0.00207, 0.00274]	4460 [4140, 4760]	0.000905 [0.00100, 0.00127]
163 ENVI (9)	0.00184 [0.00161, 0.00208]	4580 [4140, 5040]	0.000995 [0.000969, 0.00112]

I also implement a tension crack model to determine if the source could be described as a sill. The horizontal crack model gives depths deeper than the Mogi model, ranging from ~6-8km but with slightly smaller volume change rates of $\sim 1.5\text{-}3 \times 10^{-3}$ km³/yr (Table 2, Figure 12 B). The average stack length for all six tracks is ~2600m. If an aspect ratio of 1000 is assumed, the opening of the sill would correspondingly be ~2.6m. The tension crack model fits the data as well as the Mogi model, which can be seen by the comparable RMSE and by the residuals (Table 2, Figure 14 C and D).

Since the models and residuals appear remarkably similar for the Mogi model and crack model, the predicted models are differenced to determine if there is a systematic residual arising from the different deformation pattern predicted by the two models (Figure 15 A). The figure shows an insignificant difference of ~1mm/yr, and appears to be a center offset due to the effects of topography on the signal for different source depths. Both the Mogi and crack models describe the deformation equally well. However, the crack model has more degrees of freedom (dip, strike, etc.), many of which were fixed at the beginning. If these parameters had been optimized, the RMSE would likely be further reduced for the crack model.

Table 2. Tension Crack Model Results. The notation is the same as Table 1.

Track	Volume Change Rate [km ³ /yr]	Depth [m]	Length [m]	RMSE [m]
113 ERS	0.00169 [0.00166, 0.00184]	5960 [5800, 6240]	2671 [2655, 2748]	0.000723 [0.000637, 0.000756]
113 ENVI	0.00142 [0.00128, 0.00158]	7000 [6460, 7540]	2169 [2095, 2238]	0.000881 [0.000831, 0.000975]
385 ERS	0.00321 [0.00302, 0.00331]	7600 [7460, 7740]	3639 [3566, 3677]	0.000601 [0.000587, 0.000626]
385 ENVI	0.00160 [0.00140, 0.00193]	7840 [7300, 8680]	2257 [2159, 2402]	0.000626 [0.000609, 0.000677]
163 ERS	0.00206 [0.00177, 0.00235]	6620 [6160, 6920]	2664 [2535, 2786]	0.00105 [0.000991, 0.00126]
163 ENVI	0.00167 [0.00148, 0.00186]	6980 [6420, 7560]	2160 [2075, 2239]	0.000985 [0.000908, 0.00111]

Model results of a triaxial ellipsoid point source model are similar to those of the Mogi and crack models (Figure 14 E and F) [Davis, 1986]. The best fit depth ranges from ~5-6.5km with volume change rates of $\sim 1-3 \times 10^{-3}$ km³/yr (Table 3, Figure 12 C). Because the model and residuals appear similar for the ellipsoid model as well, the predicted Mogi and ellipsoid models are differenced to determine if there is another distinctive systematic residual (Figure 15 B). The figure shows that there is a slight difference of ~ 1 mm/yr, and appears to be due to the different axis ratios. The ellipsoid model produces RMSEs slightly lower than those of the Mogi and crack models. The ellipsoid model solves for the source axis ratios which allows for a better fit to the data by accounting for the slight asymmetry in the deformation. As a result, the assumption used in the crack model of an equal length and width is likely not sufficient. If the length and width were not assumed to be equal in the crack model, I would expect the RMSE to be similar to the ellipsoid model. Although the RMSE for the ellipsoid model are generally lower, they are not

significantly lower and thus not able to discriminate the model as better than the other models. The ellipsoid model should be pursued further by exploring differing angles between axes to further decrease the RMSE.

Table 3. Ellipsoid Model Results. The notation is the same as Table 1.

Track	Axis Ratios [b:a, c:a]	Volume Change Rate [km ³ /yr]	Depth [m]	RMSE [m]
113 ERS	0.6:1, 0.4:1	0.00137 [0.00135, 0.00150]	5120 [4960, 5380]	0.000714 [0.000623, 0.000749]
113 ENVI	0.1:1, 0.1:1	0.00118 [0.00106, 0.00134]	5220 [4760, 5660]	0.000843 [0.000803, 0.000921]
385 ERS	0.5:1, 0.4:1	0.00289 [0.00272, 0.00299]	6320 [6200, 6440]	0.000597 [0.000584, 0.000623]
385 ENVI	0.5:1, 0.4:1	0.00150 [0.00131, 0.00181]	6640 [6160, 7400]	0.000603 [0.000590, 0.000657]
163 ERS	0.3:1, 0.2:1	0.00158 [0.00136, 0.00179]	6120 [5680, 6420]	0.00101 [0.000931, 0.00120]
163 ENVI	0.4:1, 0.3:1	0.00150 [0.00132, 0.00169]	6340 [5800, 6900]	0.000980 [0.000905, 0.00111]

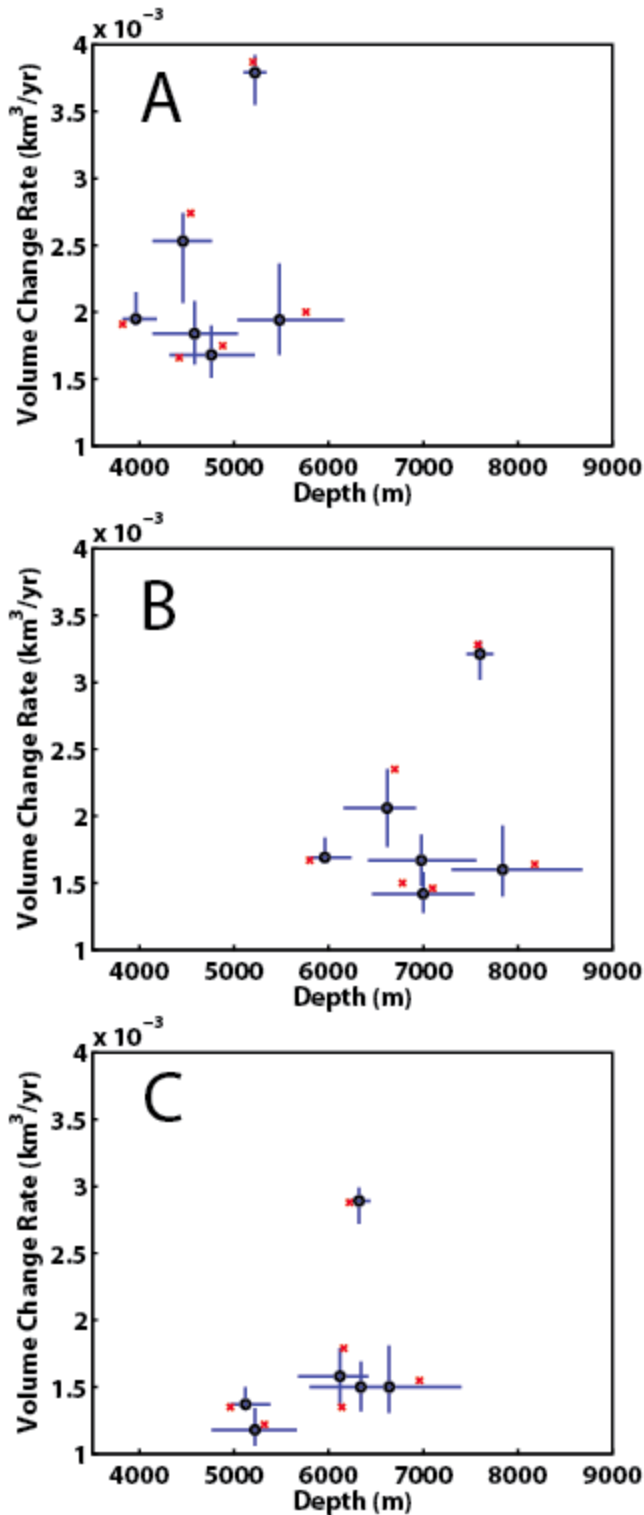


Figure 12. Model results plots. The optimal model parameters found from the inversion of InSAR stacks for A) a Mogi model B) a crack model and C) an ellipsoid model. The blue error bars depict the parameter ranges inferred from the jackknifing of interferograms in each stack. Black circles represent optimal values from stacks. Red crosses are the values for the lowest RMSE from jackknifing for each track.

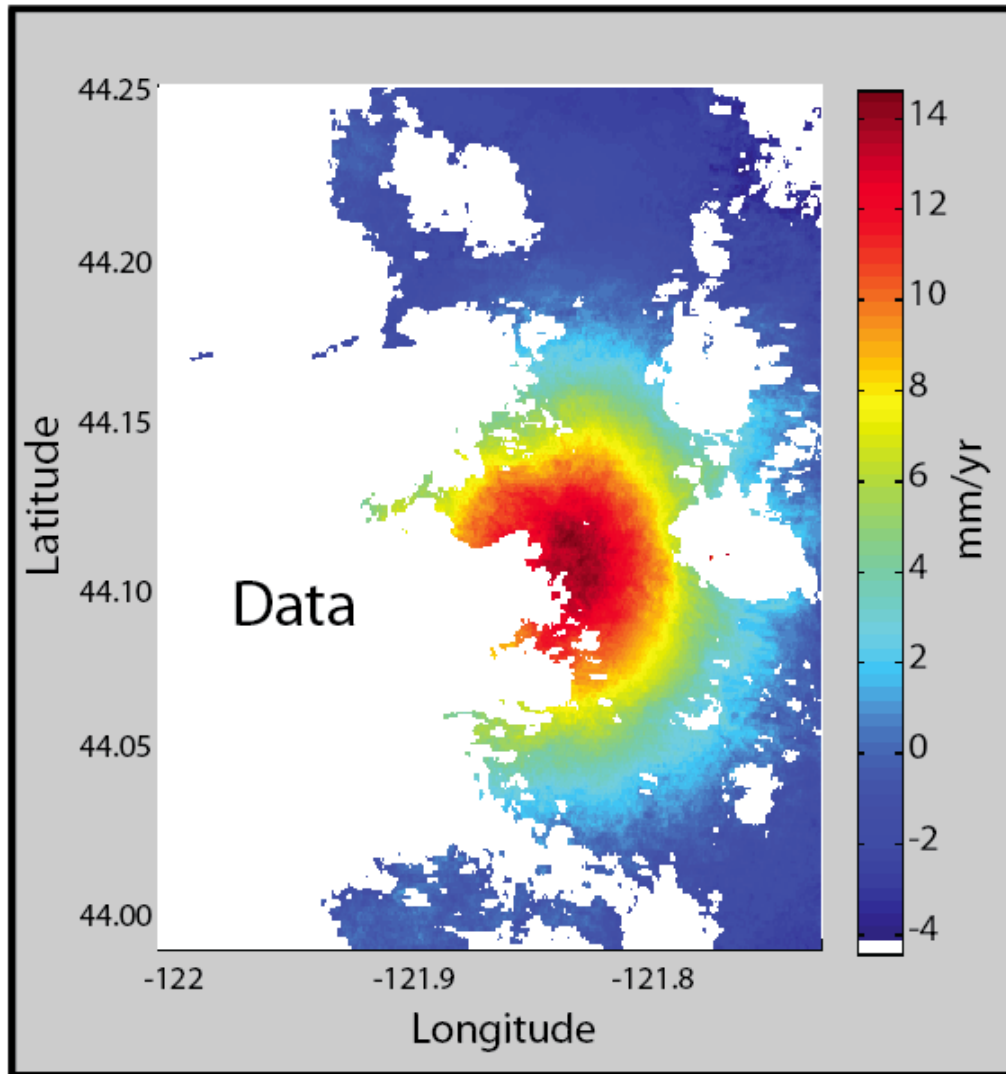


Figure 13. LOS rate for T385 ERS stack used in modeling. The stack is made from 37 interferograms spanning August 26th 1993 through August 31st 2008.

For the models using a horizontal crack, the aspect ratio of 1000 is chosen based on the physical considerations of a basaltic intrusion and by field observations. Studies that invert for sill dimensions (length or opening) from deformation data typically favor extreme maximum or minimum dimensions with very large aspect ratios of up to 2×10^6 [e.g., *Pedersen and Sigmundsson, 2004*]. However, many of these same studies also state that smaller lengths and larger openings can equally fit the data such that the total volume change is conserved. In contrast to the literature on inverse modeling, experimental and field data suggests that aspect ratios only range from <10 to 1000 [e.g., *Galland et al., 2007; Menand and Phillips, 2007; Valentine and Krogh, 2006; Hansen et al., 2011*]. The aspect ratio chosen in this study is a compromise between field data and that found from the modeling of geodetic data. Furthermore, higher aspect ratios correspond to lower viscosity composition magma, such as basalt, emplaced at several kilometers depth within the crust. It is likely that an intrusion near the Three Sisters would be basaltic to basaltic andesite, and the relatively aseismic nature of the intrusion suggests a deep source, and thus would correspond to the aspect ratios on the higher end of the experimental and field observations.

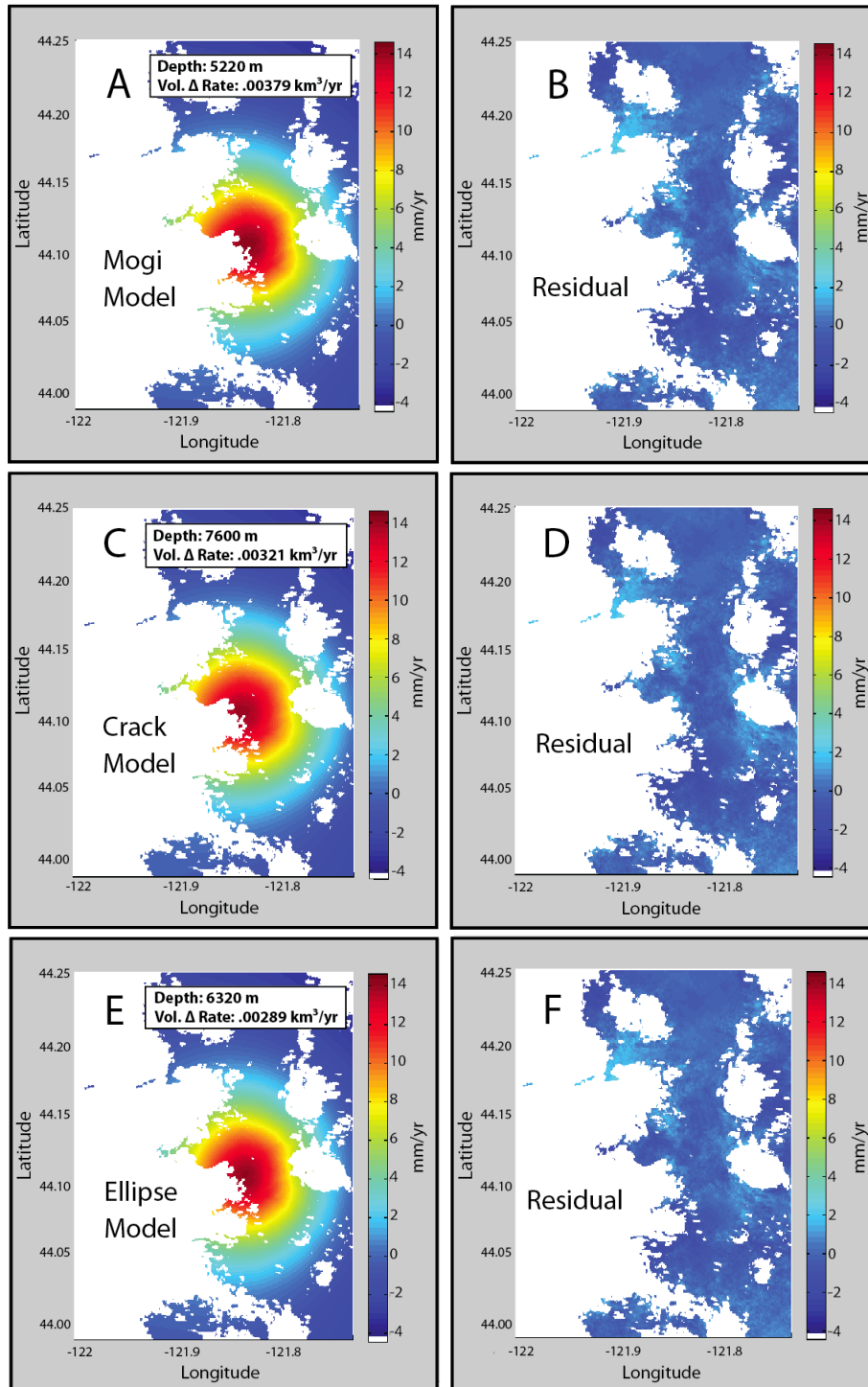


Figure 14. Model results for T385 ERS stack shown in Figure 13. The parameters used to make the above models are in the appropriate tables for the T385 ERS stack. A) The predicted Mogi model; B) The residuals from the data (Figure 13) minus the Mogi model; C) The predicted tension crack model; D) The residuals from the data minus the tension crack model; E) The predicted ellipsoid model; F) The residuals from the data minus the ellipsoidal model.

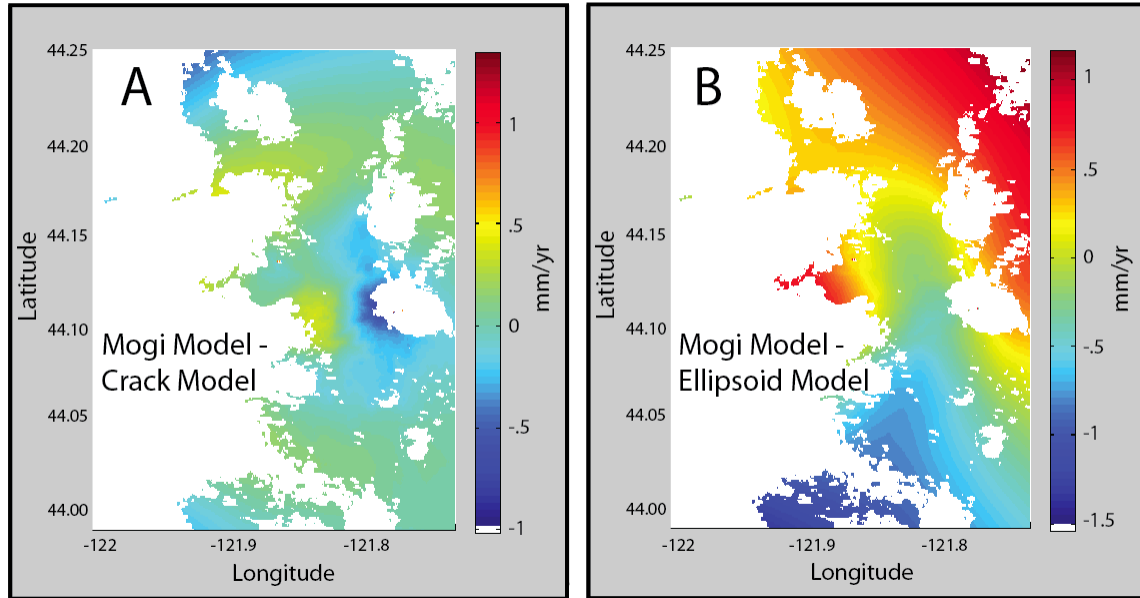


Figure 15. Predicted model differences. A) The predicted Mogi model (Figure 14 A) minus the predicted tension crack model (Figure 14 C) shows a small center offset on the scale of 1mm/yr; B) The predicted Mogi model (Figure 14 A) minus the predicted ellipsoidal model (Figure 14 E) shows a more complex difference likely from different axis ratios, but is also on the scale of 1mm/yr.

Iterations for aspect ratio, strike and dip are explored for one track to determine the optimal ranges of these previously fixed parameters. The best fit aspect ratios are low, and the deformation can be best described by ratios of 5 to 4500, with the latter value corresponding to the lowest RMSE plus five percent (Figure 16). The aspect ratio of 1000 does not vary significantly in RMSE from a very low aspect of 5, further supporting my claim that a 1000 aspect ratio is sufficient to use in modeling. The dip with the lowest RMSE is 6 degrees with a range of 1-12 degrees, and a southeast strike of 116 degrees clockwise from north with a range of 37 to 170 degrees. Ranges are based on 5% of the lowest RMSE. The strike is highly variable within a small RMSE range due to the shallow dip; in contrast, steeper dip angles would have tighter ranges due to significant reliance on strike for best fit.

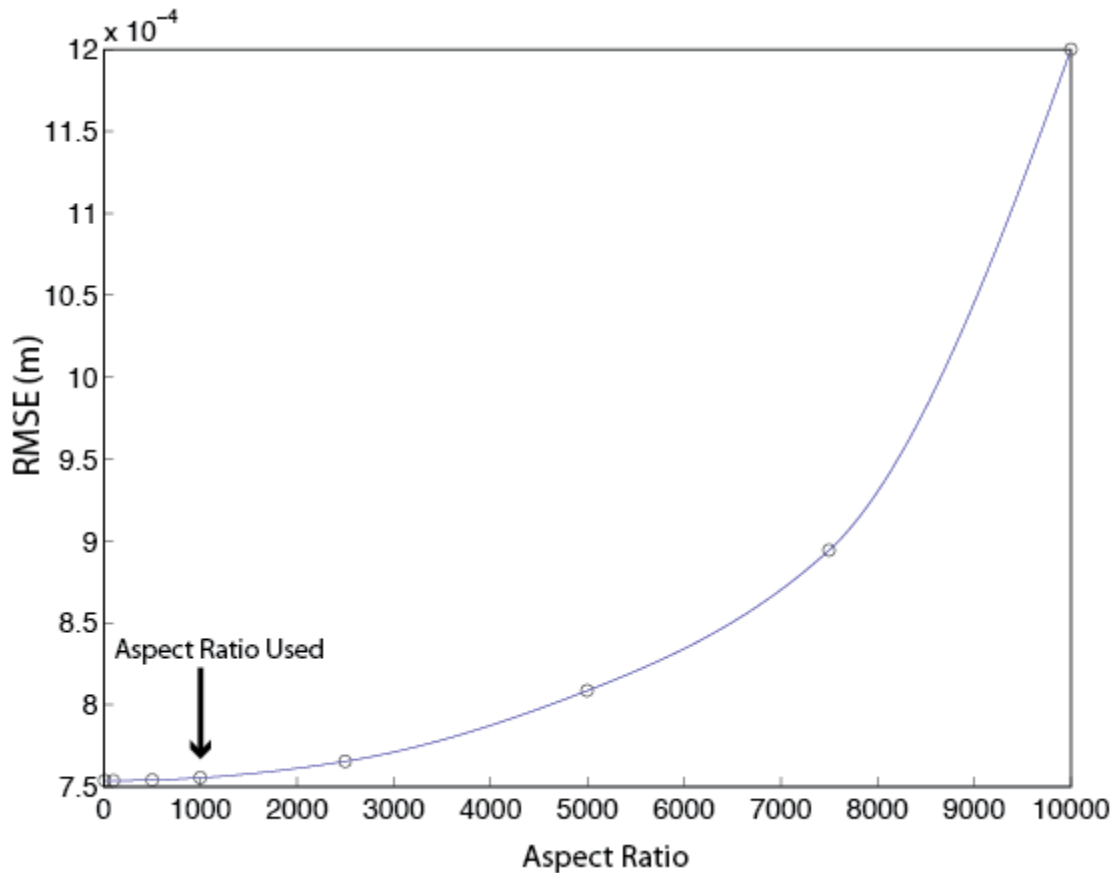


Figure 16. Experimenting with aspect ratios reveals a very small change in RMSE for aspect ratios from 1-1000. RMSE increases exponentially with aspect ratios more than a couple thousand.

Inflation Time Series

To better constrain the time-dependent inflation of a sill-like source, I invert for an inflation time series using all the best quality interferograms on different tracks. The depth of the source is assumed fixed at 7 km, which is the average crack depth of the six modeled tracks. Green's functions are calculated that relate the 3D surface deformation for a buried horizontal crack to the LOS deformation observed along each satellite track. The inflation time series shows a steady increase in volume after the summer of 1996 and then increases almost linearly from 1998 through 2004 at $\sim 7.5 \times 10^6 \text{ m}^3/\text{yr}$. A change in the slope of the time series occurs after 2004, to a more modest rate of $2 \times 10^6 \text{ m}^3/\text{yr}$

(Figure 17). The shape of the inflation curve closely matches the LOS time series as expected (Figure 7). The cumulative volume of the intrusion as of late 2010 is $6.04 \times 10^7 \text{ m}^3$. This value is the same order of magnitude of that projected by *Dzurisin et al.* [2009]. They estimate that the entire episode will have a total volume of ~ 4.5 to $5 \times 10^7 \text{ m}^3$. An intrusion of this size is relatively small, common and comparable in magnitude to other source volumes in the Aleutians [e.g., *Lu et al.*, 2002 and 2003]. The volume of the source of the Three Sisters deformation is further verified by *Dzurisin et al.* [2006], stating that the high lava production rate in the central Oregon segment of the Cascades results from relatively frequent intrusive episodes of small to moderate size. With the total volume of magma given by the inflation time series, I can also calculate the size of the sill-like source. Assuming the length and width of the crack are equal, and that the aspect ratio of length to opening is 1000, I calculate the length and width to be $\sim 3.9 \text{ km}$ with a corresponding opening of 3.9m.

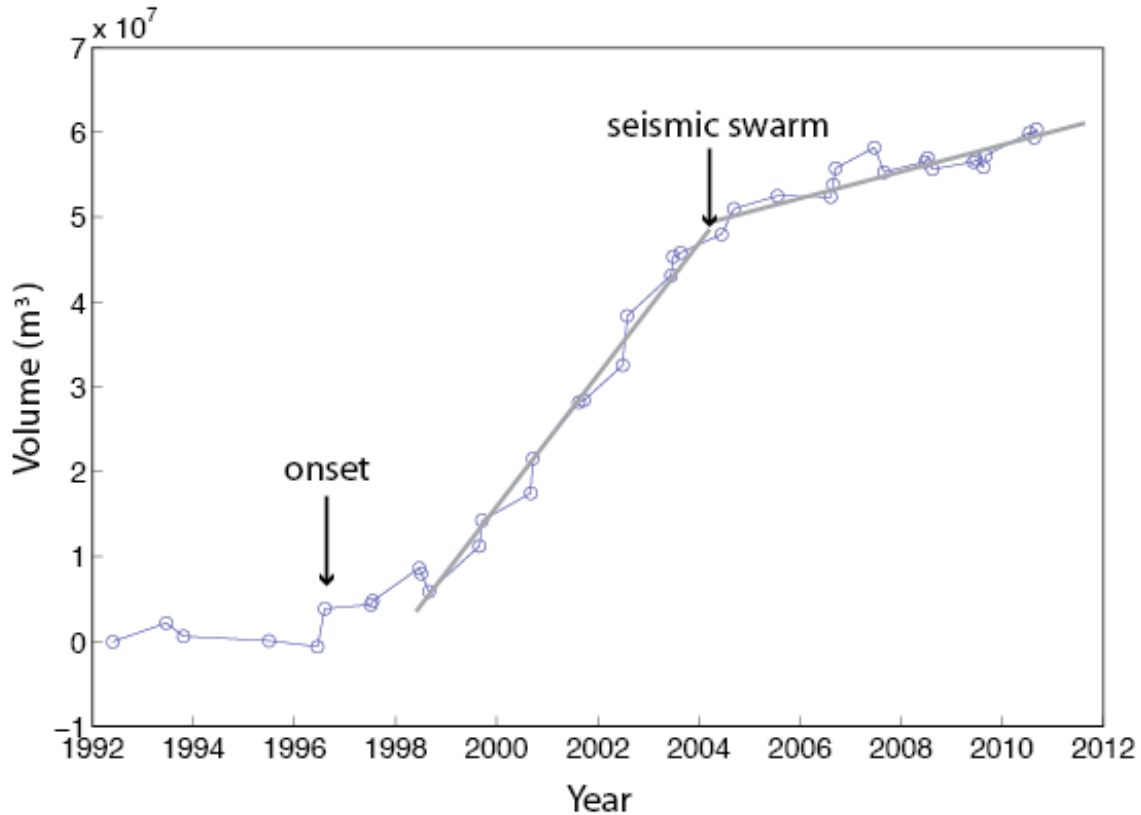


Figure 17. An inflation time series for a sill-like source combining the best data from all tracks of ERS and ENVISAT. The cumulative volume of magma injected into the sill is about $6 \times 10^7 \text{ m}^3$.

Volcanologic Interpretation

A primary purpose of this study was to learn about the Three Sisters deformation source, determine a likely source geometry that explains the deformation, and better comprehend the behavior and character of the Sisters volcanic system. Furthermore, I hoped to learn about the dynamics of Cascade volcanism, volcanic cycles, long-term emplacement of magma between major eruptions, and whether aseismic volcanic deformation is common in the Cascades or elsewhere. This study provides information on many of these topics.

Cascade volcanism has proven to be very dynamic with a diversity of behavior. The gradual and aseismic start to the deformation near the Three Sisters contrasts with

recent activity of Mount St. Helens, a volcanic system also located in the Cascades. Mount St. Helens had a rapid onset of unrest in 2004 with intense seismicity, localized surface deformation, and explosions within the first three weeks [Scott *et al.*, 2008]. This exemplifies the range of volcanic behavior within the Cascade volcanic arc, and emphasizes the importance of studying many volcanic systems within the same arc.

The Three Sisters deformation source geometry is non-unique based on the results of the three source models implemented in this study. Nevertheless, several geologic considerations suggest the source of the deformation is more likely to be a sill. The Mogi model is an idealized point source and is not physically plausible given that the true source is a finite body. The geometry of the source is also not likely to be perfectly spherical. Neither a point source nor a spherical source would likely be the actual source. Also, magma chambers of any shape, whether spherical or ellipsoidal, are now beginning to be recognized as uncommon. This is because of the special and limited conditions required to develop and maintain a magma chamber. An active magma chamber requires a delicate balance of heat in and out of the system so that a large portion of the magma reservoir could be eruptible [Menand, 2011; Gudmundsson, 1990]. Numerical simulations also show that active magma chambers can only develop with a limited range of emplacement rates [Annen, 2009]. Too low of an emplacement rate would prevent the magma chamber from developing and too high of a rate would cause an eruption that would result in increased cooling and solidification of the partially emptied magma reservoir [Menand, 2011]. In contrast, single or repeated intrusions of sills are frequent and there is a wealth of field evidence documenting these structures [Menand, 2011]. Furthermore, sills are already known to be frequent in the Three Sisters area; Williams

[1944] states that North Sister is comprised of numerous sills. Erosion has exposed hundreds of dikes and sills, many of which zigzag or are inconsistently oriented in the ediface [*Hildreth, 2007; Williams, 1944*]. Broken Top also has many mafic dikes and sills intruding its cone [*Hildreth, 2007*].

In addition to the geologic predominance of sills, the lack of seismicity associated with the inflation is consistent with the deeper source depth found for the sill model. For the deformation to be aseismic, the source would need to be deep enough to be below the brittle-ductile transition, which is thought to be as shallow as 5km depth beneath active volcanoes [*Hill, 1992*]. Most of the Mogi model results are shallower than 5km and the ellipsoidal results extend to ~6.5km. If magma was injected to this shallow level, I would have expected greater seismicity in the region during the intrusion. The sill depths for each track are all deeper than 5km, with an average of 7km. The one swarm of earthquakes in 2004 is likely due to stress build up in the upper crust from the continual inflation over ~8 years or volatiles rising off of the intrusion. The crust relieved some of the accumulated stress by means of the earthquake swarm along favorably oriented faults several kilometers away from the source center. The seismic swarm may be related to the distinct change in slope in the inflation time series after 2004 and may have marked a change in the dynamics of the intrusion. It is impossible to tell, however, if the swarm changed the dynamics of the intrusion, or if a change in the pressure, rate, etc. of the intrusion caused the seismic swarm. Nonetheless, there is a possible connection between the deformation and the seismicity.

Aseismic intrusions are fairly common in other volcanic arcs. *Wicks et al.* [2002] note that aseismic inflation has been observed at two volcanoes in the Aleutian arc,

Westdahl and Peulik [Lu *et al.*, 2000, 2002]. The Peulik inflation episode is comparable to the Three Sisters, with a similar source depth at ~7km, and about the same volume of ~0.05km³ [Lu *et al.*, 2002]. Furthermore, Peulik also experienced one seismic swarm during the event; although it is not clear whether it was directly related to the volcanic inflation since the swarm occurred ~30km from the deformation [Lu *et al.*, 2002]. The Three Sisters deformation differs in that it is much longer lived, while Peulik deformation lasted only a few years. The earthquake swarm at the Three Sisters was smaller in magnitude, with the greatest earthquake of a moment magnitude of 1.9 [Dzurisin *et al.*, 2006]. Aseismicity is common in the Aleutians but is also thought to be common elsewhere in the Cascades. Lu *et al.* [2002] use evidence from Mount St. Helens to support the idea that aseismic intrusions are likely to be relatively common with magma accumulating gradually and preferentially near the brittle-ductile transition depth in the crust. They state that the magma beneath Mount St. Helens accumulated aseismically at about 7km depth prior to the 1980 eruption [Lu *et al.*, 2002].

Data from melt inclusions collected at Collier Cone and Four-in-One Cone near North Sister give mid to upper-crustal magma storage depths. Melt inclusions are small trapped pockets of primitive melt in crystals of erupted products that provide information on the magma at depth prior to eruption. By analyzing these inclusions, one can determine the composition, volatile content, and the pressure of equilibration of the magma, which can then be related to the depth of magma storage. The melt inclusions of the cinder cones near North Sister suggest that magma is commonly stored at 100-200MPa, which corresponds to depths of ~4-8km [Ruscitto *et al.*, 2010]. However, these results are considered minima due to CO₂-rich vapor bubbles within the melt inclusions,

and likely the storage depth would be the upper range of 6-8km [pers. comm. Ruscitto]. These results thus favor the deeper depths given by the sill model and also provide verification that the model results agree with the geology of the Three Sisters area. Furthermore, this equilibration depth is similar to that found elsewhere in the Cascades, such as at Mount St. Helens where data indicate a source depth of at least 7km for material erupted in May 1980 [Pallister *et al.*, 1992]. Two independent earthquake studies show an aseismic magma source region between 7-14km and 6.5-10km beneath Mt. St. Helens [Scandone and Malone, 1985; Moran, 1994]. The 1980 Mt. St. Helens erupted pumice's mineral assemblage was similarly determined to have equilibrated at about 7.2km depth [Rutherford *et al.*, 1985]. This may imply a common preferential depth for a brittle-ductile transition zone beneath Mount St. Helens and the Three Sisters at about 7-10km depth.

Inflation episodes not culminating in an eruption may be common in the Cascade volcanic arc. The periodic long-term emplacement of magma is likely part of the volcanic cycle and is vital to the life cycle of volcanoes for recharging the system. Dzurisin *et al.* [2006] speculate that intrusive episodes last from days to years and are separated by quiescent periods of tens-to-hundreds of years. Melt at depth is fed to a mid to upper-crustal source via dikes in episodic surges. If these intrusions of magma are closely spaced in time, this can keep the previous pulse of melt from solidifying and allow for magma to accumulate. When enough magma has accumulated through several intrusions, and a threshold is reached, an eruption could take place. The Three Sisters area should be continually monitored, especially if this intrusion continues or if another intrusion occurs within several years of this episode. Geochemical evidence from springs of the Three

Sisters area indicate that this intrusive episode is likely the latest in a series of magma intrusions [Wicks *et al.*, 2002]. Intrusions such as these likely occur frequently in the Cascades but can elude detection due to their aseismic nature.

Successive, independent intrusions of sills have been called upon to explain magma body formation and growth, including the building of large plutons [Menand, 2011]. Sills are becoming widely recognized as the building blocks in laccolith and pluton formation, especially as seen in field evidence for mid to upper-crustal depths [Menand, 2011]. If the Three Sisters intrusion is one of several, and there is enough time between intrusions to allow for solidification, it could be in the process of forming a laccolith or lopolith. Sills form mainly due to rheology contrasts, rigidity anisotropy, and rotation of deviatoric stress [e.g., Menand, 2011; Parsons *et al.*, 1992; Kavanagh *et al.*, 2006]. Once the first sill forms from the dominant mechanism, the emplaced sill creates a rigidity contrast with the surrounding rock that would provide a favorable site for future sill emplacement [Menand, 2011]. This creates a vertical stacking of sills, which is thought to explain the formation of internally-layered laccoliths, plutons, and Christmas-tree laccoliths [Menand, 2011]. Thus, sill-like intrusions in the Three Sisters area could be forming or adding to an extensive intrusive complex.

The ongoing deformation is clearly offset from the Three Sisters stratovolcanoes. It is likely that the deformation is from an intrusion unrelated to the Three Sisters volcanoes, and if erupted, would produce a cinder cone, since most activity in the Cascades is due to mafic shields and cones [Hildreth, 2007]. Hildreth [2007] also comments that nowhere else in the Cascades “are vent alignments more conspicuous than in this reach, where lines of mafic volcanoes (and even chains of rhyolite vents) form

several north-trending arrays.” It is plausible that the current deformation sits above a zone of weakness within the high Cascades graben and that these north-south zones of weakness are likely responsible for many of the cinder cone chains in the region.

Although I conclude that the deformation near Three Sisters is likely due to a single tabular basaltic sill, realistically it may be much more complex. *Williams* [1944] states that the numerous sills exposed on North Sister “branch, pinch, and swell in a confused manner.” The recent intrusion probably adds to a pre-existing extensive intrusive complex and is unclear whether the successive intrusions could culminate in an eruption or instead form a laccolith or lopolith by amalgamation of successive injections.

StaMPS Assessment

StaMPS is the first PS technique designed to work in rural areas. Since StaMPS has never been applied to the Cascades, I provide an assessment on how well StaMPS performs in this area. The statistical algorithms identify surface features that exhibit time invariant scattering characteristics and a bright backscatter response. StaMPS specifically uses the spatial correlation of interferometric phase to find pixels with a low phase variance [*Hooper et al.*, 2007]. Other PS techniques rely solely on amplitude and require a model of how the deformation varies in time [e.g., *Ferretti et al.*, 2001; *Lyons and Sandwell*, 2003]. StaMPS is also unique in that it does not require any previous knowledge of the deformation rates [*Hooper et al.*, 2007].

The selection of persistent scatterers is a statistical process, and thus some false positives are expected. Here I assess the selection of scatterers by comparing the location of scatterers to surface characteristics. StaMPS processing chooses thousands of PS

pixels on all tracks. Figure 18 reveals that scatterers correspond very well with the rocky, stable surface provided by lava flows. Few scatterers are chosen in dense vegetation, water, or snow covered areas, as expected. Scatterers around lakes near the Three Sisters appear mostly on andesite blocks and not in the lakes or surrounding forest (Figure 19 A). No scatterers are found over scree slopes where loosely consolidated tephra is reconfigured beneath the winter snowpack (Figure 19 B). Field investigation shows that some scatterers were picked on blocky lava flows with scattered underbrush (Figure 20). When it comes to assessing the accuracy of the LOS signal, the StaMPS LOS velocity is consistent with the stack LOS velocity (Figure 18). Underbrush did not appear to affect the scatterers chosen by StaMPS, whereas forests proved problematic. The StaMPS time series generally agree with the small-baseline and GPS time series; they all are about the same order of magnitude of deformation and exhibit similar trends (Figure 7 and 9).

Although StaMPS picks scatterers accurately, the phase change has shown to be more inconsistent. Common problems with the phase include ramps and noise. Most of the StaMPS results have extremely large orbital ramps upwards of tens of centimeters of range-change across the scene. Using the option to remove orbital ramps typically worked well, but smaller ramps sometimes remained in the images. Small magnitude noise existed in all images. The StaMPS results for a non-deforming epoch sometimes had several centimeters of random range-change. I attempted modifying many of the StaMPS parameters to smooth the noise but was not successful.

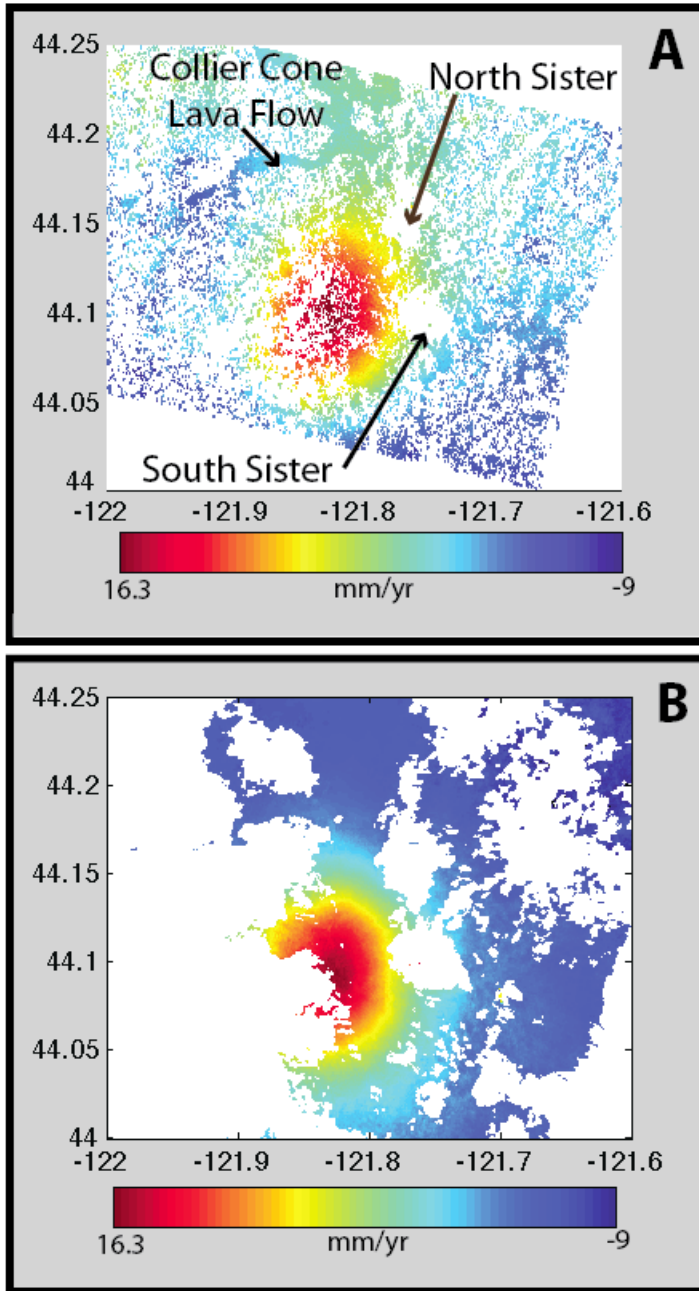


Figure 18. StaMPS and stack comparison. A) StaMPS mean LOS velocity for T385 ERS from July 13th 1995 to September 7th 2003. Each dot represents a persistent scatterer, with the greatest density of scatterers found on sparsely vegetated lava flows. B) Stack of interferograms showing mean LOS velocity. This image is the same track and dates as the StaMPS mean LOS velocity in A for a direct comparison. This demonstrates how large patches of the region are decorrelated with standard interferometry.

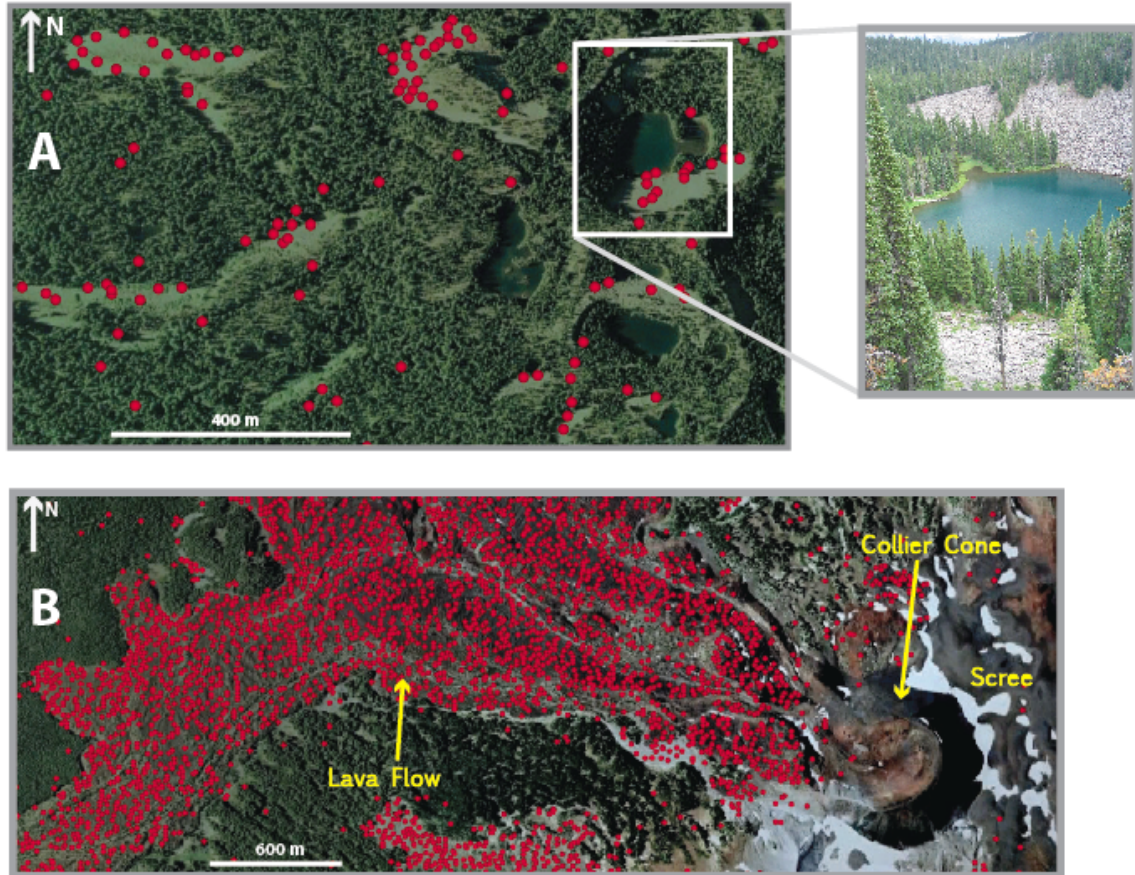


Figure 19. T113 ERS Persistent scatterers picked by StaMPS over select areas. Ground features match very well with the chosen scatterers. A) PS pixels are concentrated on stable scree slopes of 0.1-1m andesitic blocks; B) PS picked over Collier cone. The cone itself has few PS pixels due to loosely consolidated material that easily changes properties each year from snow. The lava flows are more stable and have an abundance of PS pixels.

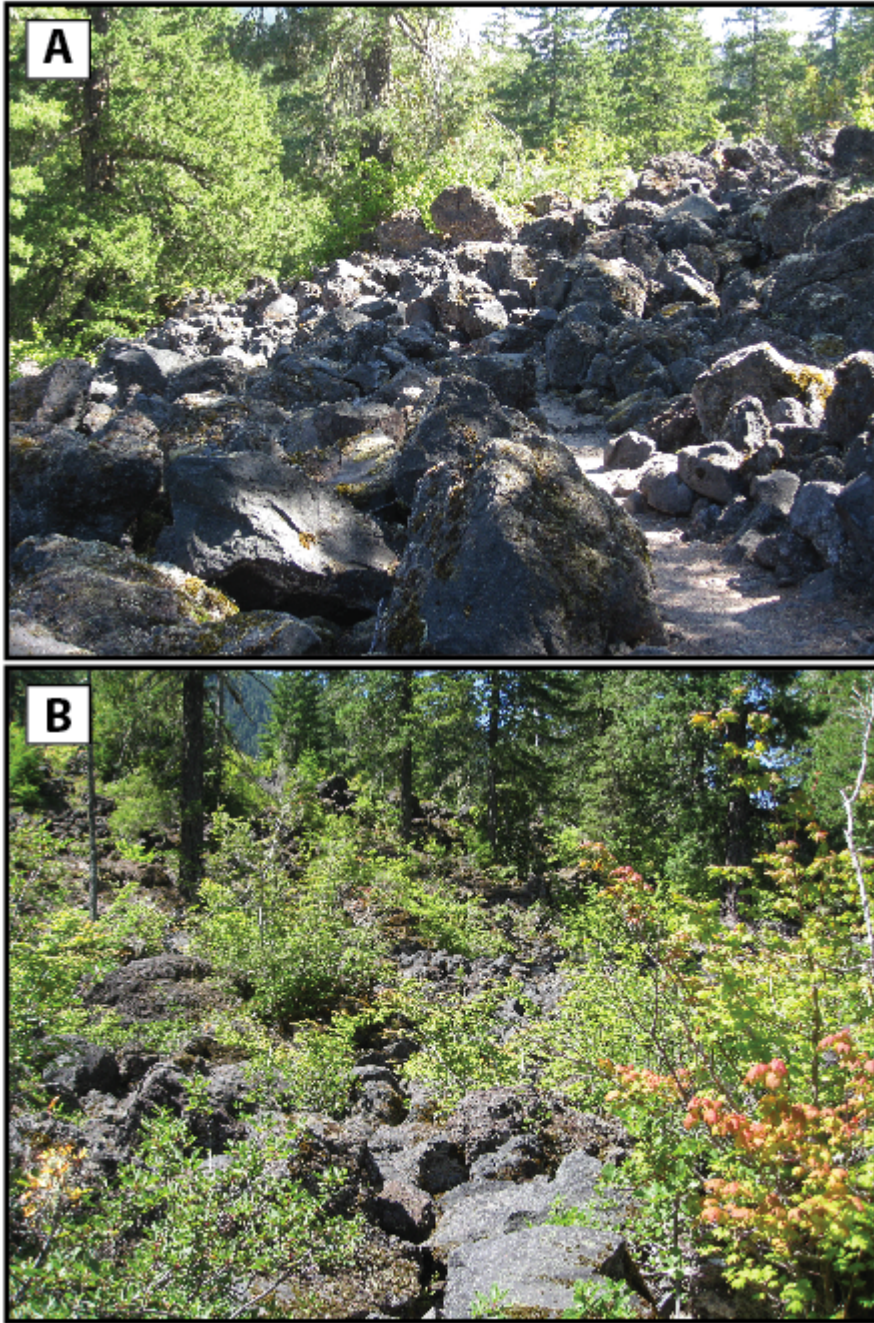


Figure 20. Field photos. A) PS pixels were chosen for this area of blocky lava flows with no vegetation; B) PS pixels were also chosen for this area of the same flow but with dispersed vegetation.

CHAPTER V

CONCLUSIONS

I used single interferograms, stacks, LOS time series, inflation time series, and modeling to examine volcanic deformation near Three Sisters, Oregon. I interpret the deformation to be caused by the intrusion of magma at depth, resulting in ~25 cm range-change through 2010. The deformation began between late summer of 1996 and summer of 1997. Uplift started gradually and increased to ~3-4.5 cm/yr from 1998 through 2003. A marked decrease to ~25% of the inflation rate occurred after 2004 and continues through 2010. This change in intrusion behavior may be related to the seismic swarm that occurred in March of 2004. In 2010, the deformation rate is near the magnitude of the noise, but appears to be about 6-8 mm/yr.

I explore the source of the deformation by modeling the InSAR data assuming a Mogi point source, a tension crack, and an ellipsoidal pressure source. All models describe the deformation equally well based on the fit to the data. Based on geologic considerations, I hypothesize that the source is likely a sill of basalt with a length of approximately 3900m and an opening of 3.9m at a depth of 7000m. The sill model gives deeper depths than the Mogi and ellipsoid models. A deeper source seems more probable due to the lack of seismicity from the inflation. Sills are also common in the Three Sisters area and the source of deformation is more likely sill-like than the other model geometries. The total volume of magma intruded as of 2010 is $\sim 6 \times 10^7 \text{ m}^3$, which is comparable in size to other modeled sills and other sources in the Aleutians.

StaMPS successfully picked thousands of persistent scatterers within the dense vegetation of the Cascades. The scatterers were mainly over areas dominated by boulders

or lava flows and not in areas with unstable scree slopes, dense forest, water, or seasonal snow cover. However, the phase signal determined by StaMPS is more complex and the results for different tracks are somewhat inconsistent. Ramps and/or random noise are found in each run. I hypothesize that StaMPS would perform better if the signal to noise were larger than observed. More experimentation is needed with StaMPS before a final assessment can be made for the Cascades. Overall, the StaMPS time series appeared consistent with the small-baseline time series and GPS time series. My results demonstrate that StaMPS has the potential to resolve a more complete deformation signal in mountainous regions that would otherwise be decorrelated in traditional interferometry.

APPENDIX

ACRONYM TABLE

ALOS	Advanced Land Observation Satellite
DEM	Digital Elevation Model
DLP	Deep Long Period earthquake
ENVISAT	ENVironmental SATellite
ERS	European Remote Sensing satellite
GPS	Global Positioning System
InSAR	Interferometric Synthetic Aperture Radar
LOS	Line Of Sight
PS	Persistent Scatterer
RMSE	Root Mean Square Error
ROI PAC	Repeat Orbit Interferometry Package
SAR	Synthetic Aperture Radar
SNAPHU	Statistical-cost, Network-flow Algorithm for Phase Unwrapping
SRTM	Shuttle Radar Topography Mission
StaMPS	Stanford Method for Persistent Scatterers
USGS	United States Geological Survey
WInSAR	Western North America InSAR

REFERENCES CITED

- Annen, C. (2009), From plutons to magma chambers: thermal constraints on the accumulation of eruptible silicic magma in the upper crust, *Earth Planet. Sci. Lett.*, 284, 409–416.
- Chen, C.W. and H.A. Zebker (2002), Phase unwrapping for large SAR interferograms: Statistical segmentation and generalized network models, *IEEE Trans. Geosci. Remote Sens.*, 40, 1709–1719.
- Davis, P.M. (1986), Surface deformation due to inflation of an arbitrarily oriented triaxial ellipsoidal cavity in an elastic half-space, with reference to Kilauea Volcano, Hawaii, *J. Geophys. Res.*, 91, 7429–7438.
- Dzurisin, D., M. Lisowski, C.W. Wicks, M.P. Poland, and E.T. Endo (2006), Geodetic observations and modeling of magmatic inflation at the Three Sisters volcanic center, central Oregon Cascade Range, USA. *J. Volcanol. Geotherm. Res.*, 150, 35–54.
- Dzurisin, D., M. Lisowski, and C.W. Wicks (2009), Continuing inflation at Three Sisters volcanic center, central Oregon Cascade Range, USA, from GPS, leveling, and InSAR observations, *Bull. Volcanol.*, 71, 1091–1110.
- Ewert, J.W., M. Guffanti, and T.L. Murray (2005), An Assessment of Volcanic Threat and Monitoring Capabilities in the United States – Framework for a National Volcanic Early Warning Systems (NVEWS), USGS Open-File Report 2005-1164.
- Farr, T.G., and M. Kobrick (2000), Shuttle Radar Topography Mission produces a wealth of data, *Eos Trans. AGU*, 81, 583–585.
- Ferretti, A., C. Prati, and F. Rocca (2000), Nonlinear subsidence rate estimation using permanent scatterers in differential SAR interferometry, *IEEE Trans. Geosci. Remote Sens.*, 38, 2202–2212.
- Ferretti, A., C. Prati, and F. Rocca (2001), Permanent scatterers in SAR interferometry, *IEEE Trans. Geosci. Remote Sens.*, 39, 8–20.
- Galland, O., P.R. Cobbold, J. de Bremond d’Ars, and E. Hallot (2007), Rise and emplacement of magma during horizontal shortening of the brittle crust: Insights from experimental modeling, *J. Geophys. Res.*, 112, B06402.
- Grandin, R., A. Socquet, M.P. Doin, E. Jacques, J.B. de Chabalier, and G.C.P. King (2010), Transient rift opening in response to multiple dike injections in the Manda Hararo rift (Afar, Ethiopia) imaged by time - dependent elastic inversion of interferometric synthetic aperture radar data, *J. Geophys. Res.*, 115, B09403.

- Gudmundsson, A. (1990), Emplacement of dikes, sills and crustal magma chambers at divergent plate boundaries, *Tectonophysics*, 176, 257-275.
- Hansen, J., D.A. Jerram, K. McCaffrey, and S.R. Passey (2011), Early Cenozoic saucer-shaped sills of the Faroe Islands: an example of intrusive styles in basaltic lava piles, *J. Geol. Soc. London*, 168, 159-178.
- Hildreth, W. (2007), Quaternary Magmatism in the Cascades-Geologic Perspectives, *U.S. Geol. Surv. Prof.*, 1744.
- Hill, D.P. (1992), Temperatures at the base of the seismogenic crust beneath Long Valley caldera, California, and the Phlegrean Fields caldera, Italy in *Volcanic Seismology, IAVCEI Proc. Volcanol.*, vol. 3, edited by P. Gasparini et al., pp. 433-461, Springer-Verlag, New York.
- Hooper, A., P. Segall, and H. Zebker (2007), Persistent scatterer InSAR for crustal deformation analysis, with application to Volcan Alcedo, Galapagos, *J. Geophys. Res.*, 112, B07407.
- Hooper, A. (2008), A multi-temporal InSAR method incorporating both persistent scatterer and small baseline approaches, *Geophys. Res. Lett.*, 35, L16302.
- Kavanagh, J.L., T. Menand, and R.S.J. Sparks (2006), An experimental investigation of sill formation and propagation in layered elastic media, *Earth Planet. Sci. Lett.*, 245, 799–813.
- Lu, Z., C. Wicks, D. Dzurisin, W. Thatcher, J.T. Freymueller, S.R. McNutt, and D. Mann (2000), Aseismic Inflation of Westdahl volcano, Alaska, revealed by satellite radar interferometry, *Geophys. Res. Lett.*, 27, 1567–1570.
- Lu, Z., C. Wicks Jr., D. Dzurisin, J.A. Power, S.C. Moran, and W. Thatcher (2002), Magmatic inflation at a dormant stratovolcano: 1996-1998 activity at Mount Peulik volcano, Alaska, revealed by satellite radar interferometry, *J. Geophys. Res.*, 107(B7), 2134.
- Lu, Z., T. Masterlark, D. Dzurisin, R. Rykhus, and C. Wicks Jr. (2003), Magma supply dynamics at Westdahl volcano, Alaska, modeled from satellite radar interferometry, *J. Geophys. Res.*, 108(B7), 2354.
- Lyons, S., and D. Sandwell (2003), Fault creep along the southern San Andreas from interferometric synthetic aperture radar, permanent scatterers, and stacking, *J. Geophys. Res.*, 108(B1), 2047.
- McCaffrey, R.M., M.D. Long, C. Goldfinger, P.C. Zwick, J.L. Nabelek, C.K. Johnson, and C. Smith (2000), Rotation and plate locking at the southern Cascadia subduction zone, *Geophys. Res. Lett.*, 27, 3117–3120.

- Menand, T., and J.C. Phillips (2007), Gas segregation in dykes and sills, *J. Volcanol. Geotherm. Res.*, 159, 393–408.
- Menand, T. (2011), Physical controls and depth of emplacement of igneous bodies: A review, *Tectonophysics*, 500, 11–19.
- Miller, R.G. (1974), The jackknife—a review, *Biometrika*, 61, 1–15.
- Mogi, K. (1958), Relations between the eruptions of various volcanoes and the deformations of the ground surfaces around them, *Bull. Earthquake Res. Inst. Univ. Tokyo*, 36, 99–134.
- Moran, S.C. (1994), Seismicity at Mount St. Helens, 1987-1992: Evidence for repressurization of an active magmatic system, *J. Geophys. Res.*, 99, 4341–4354.
- Moran, S.C. (2004), Seismic Monitoring at Cascade Volcanic Centers, 2004—Status and Recommendations, *U.S. Geol. Surv. Invest. Rep.*, 2004–5211.
- Nichols, M.L., S.D. Malone, S.C. Moran, W.A. Thelen, and J.E. Vidale (2011), Deep long-period earthquakes beneath Washington and Oregon volcanoes, *J. Volcanol. Geotherm. Res.*, 200, 116–128.
- Pallister, J.S., R.P. Hoblitt, D.R. Crandell, and D.R. Mullineaux (1992), Mount St. Helens a decade after the 1980 eruptions: magmatic models, chemical cycles, and a revised hazards assessment, *Bull. Volcanol.*, 54, 126–146.
- Parsons, T., N.H. Sleep, and G.A. Thompson (1992), Host rock rheology controls on the emplacement of tabular intrusions: implications for underplating of extending crust, *Tectonics*, 11, 1348–1356.
- Pedersen, R., and F. Sigmundsson (2004), InSAR based sill model links spatially offset areas of deformation and seismicity for the 1994 unrest episode at Eyjafjallajökull volcano, Iceland, *Geophys. Res. Lett.*, 31, L14610.
- Rosen, P.A., S. Hensley, I.R. Joughin, F.K. Li, S.N. Madsen, E. Rodriguez, and R.M. Goldstein (2000), Synthetic aperture radar interferometry, *Proc. IEEE*, 88, 333–382.
- Rosen, P.A., S. Henley, G. Peltzer, and M. Simons (2004), Updated repeat orbit interferometry package released, *Eos Trans. AGU*, 85, 47.
- Ruscitto, D.M., P.J. Wallace, E.R. Johnson, A.J.R. Kent, and I.N. Bindeman (2010), Volatile contents of mafic magmas from cinder cones in the Central Oregon High Cascades: Implications for magma formation and mantle conditions in a hot arc, *Earth Planet. Sci. Lett.*, 298, 153–161.

- Rutherford, M.J., H. Sigurdsson, S. Carey, and A. Davis (1985), The May 18, 1980, eruption of Mount St. Helens 1. Melt composition and experimental phase equilibria, *J. Geophys. Res.*, *90*, 2929–2947.
- Sandwell, D.T., and E. Price (1998), Phase gradient approach to stacking interferograms, *J. Geophys. Res.*, *103*, 30183–30204.
- Scandone, R. and S.D. Malone (1985), Magma supply, magma discharge and readjustment of the feeding system of Mount St. Helens during 1980, *J. Volcanol. Geotherm. Res.*, *23*, 239–262.
- Schmidt, D. A., and R. Bürgmann (2003), Time-dependent land uplift and subsidence in the Santa Clara valley, California, from a large interferometric synthetic aperture radar data set, *J. Geophys. Res.*, *108* (B9), 2416.
- Schmidt, M.E. and A.L. Grunder (2011), Deep Mafic Roots to Arc Volcanoes: Mafic Recharge and Differentiation of Basaltic Andesite at North Sister Volcano, Oregon Cascades, *J. Petrology*, *52*, 603–641.
- Scott, W.E., and C.A. Gardner (1990), Field trip guide to the central Oregon High Cascades: part 1, Mount Bachelor-South Sister area. *Or. Geol.*, *52*, 99–114.
- Scott, W.E., R.M. Iverson, S.P. Schilling, and B.J. Fisher (2001), Volcano hazards in the Three Sisters region, Oregon, *U.S. Geol. Surv. Open-File Report*, 99–437.
- Scott, W.E., D.R. Sherrod, and C.A. Gardner (2008), Overview of the 2004 to 2006, and Continuing, Eruption of Mount St. Helens, Washington, in *A volcano rekindled: The renewed eruption of Mount St. Helens, 2004-2006*, edited by D.R. Sherrod et al., *U.S. Geol. Surv. Prof Pap.*, *1750*, 3–22.
- Sherrod, D.R., and J.G. Smith (1990), Quaternary extrusion rates of the Cascade Range, northwestern United States and southern British Columbia, *J. Geophys. Res.*, *95*, 19465–19474.
- Sherrod, D.D., E.M. Taylor, M.L. Ferns, W.E. Scott, R.M. Conrey, and G.A. Smith (2004), Geologic map of the Bend 30- by 60- minute quadrangle, central Oregon, Map I-2683, U.S. Geological Survey, Washington, D.C..
- Taylor, E.M. (1981), Central High Cascade roadside geology, Bend, Sisters, McKenzie Pass, and Santiam Pass, Oregon, in *Guides to some volcanic terranes in Washington, Idaho, Oregon, and northern California*, edited by D.A. Johnston and J.M. Donnelly-Nolan, *U.S. Geol. Surv. Circ.*, *838*, 55–58.
- Valentine, G.A, and K.E.C. Krogh (2006), Emplacement of shallow dikes and sills beneath a small basaltic volcanic center – The role of pre-existing structure (Paiute Ridge, souther Nevada, USA), *Earth Planet. Sci. Lett.*, *246*, 217–230.

- Wicks, C.W. Jr, D. Dzurisin, S. Ingebritsen, W. Thatcher, Z. Lu, and J. Iverson (2002), Magmatic activity beneath the quiescent Three Sisters volcanic center, central Oregon Cascade Range, USA. *Geophys Res Lett*, 29, 1122.
- Williams, H. (1944), Volcanoes of the Three Sisters region, Oregon Cascades, *Univ. Calif. Pub.*, 27, 37–84.
- Williams, C.A., and G. Wadge (1998), The effects of topography on magma chamber deformation models: Application to Mt. Etna and radar interferometry, *Geophys. Res. Lett.*, 25, 1549–1552.
- Williams, C. A., and G. Wadge (2000), An accurate and efficient method for including the effects of topography in three-dimensional elastic models of ground deformation with applications to radar interferometry, *J. Geophys. Res.*, 105(B4), 8103–8120.
- Yang, X. and P.M. Davis (1986), Deformation due to a rectangular tension crack in an elastic half-space, *Bull. Seism. Soc. Am.*, 76, 865–881.
- Zebker, H.A. and J. Villasenor (1992), Decorrelation in interferometric radar echoes, *IEEE Trans. Geosci. Remote Sensing*, 30, 950–959.
- Zebker, H.A., P.A. Rosen, and S. Hensley (1997), Atmospheric effects in interferometric synthetic aperture radar surface deformation and topographic maps, *J. Geophys. Res.*, 102, 7547–7563.